Cell Stem Cell

Article

Structural and functional integration of human forebrain organoids with the injured adult rat visual system

Graphical abstract

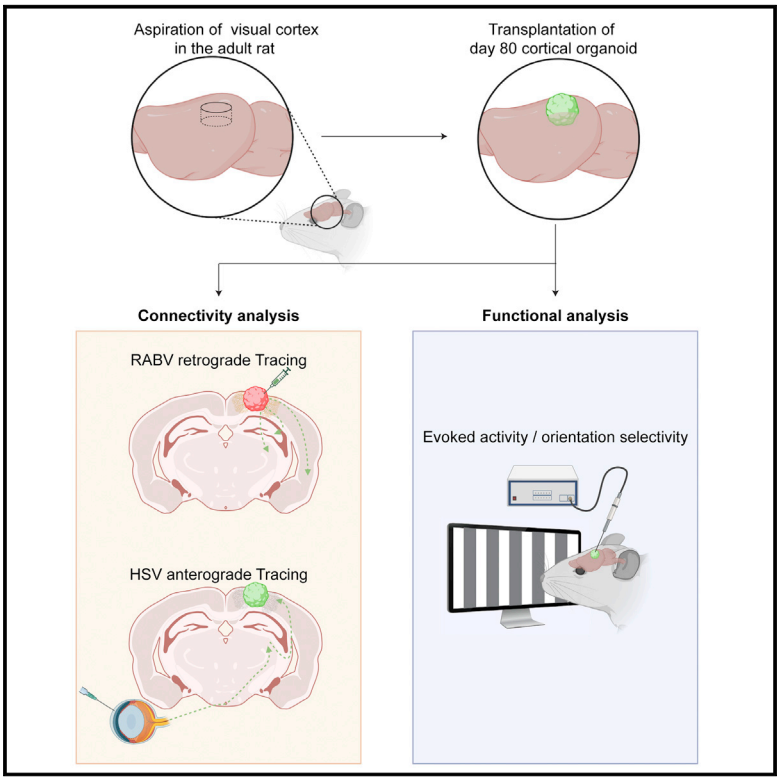

Highlights

- Human brain organoids integrate with the injured visual cortex of adult rats
- Organoid grafts are synaptically connected to the host retina and visual system
- Organoid neurons respond to host visual stimulation and adopt feature selectivity

Authors

Dennis Jgamadze, James T. Lim, Zhijian Zhang, ..., Hongjun Song, Guo-li Ming, Han-Chiao Isaac Chen

Correspondence

isaac.chen@pennmedicine.upenn.edu

In brief

Chen and colleagues demonstrate that human brain organoids can integrate structurally and functionally with the injured adult mammalian brain. Organoid grafts connect synaptically with the rat brain and adopt the function of the visual cortex. These findings support brain organoid transplantation as a therapeutic strategy for restoring cortical function.

Jgamadze et al., 2023, Cell Stem Cell *30*, 137–152
February 2, 2023 Published by Elsevier Inc.
https://doi.org/10.1016/j.stem.2023.01.004

CellPress

Cell Stem Cell

CellPress

Article

Structural and functional integration of human forebrain organoids with the injured adult rat visual system

Dennis Jgamadze,[1] James T. Lim,[1] Zhijian Zhang,[2] Paul M. Harary,[1] James Germi,[1] Kobina Mensah-Brown,[1] Christopher D. Adam,[1] Ehsan Mirzakhalili,[1] Shikha Singh,[1] Jiahe Ben Gu,[1] Rachel Blue,[1] Mehek Dedhia,[1] Marissa Fu,[3] Fadi Jacob,[2] Xuyu Qian,[2] Kimberly Gagnon,[1] Matthew Sergison,[1] Oceane Fruchet,[1] Imon Rahaman,[1] Huadong Wang,[4,12] Fuqiang Xu,[4,5,12] Rui Xiao,[6] Diego Contreras,[2] John A. Wolf,[1,7] Hongjun Song,[2,8,9,10] Guo-li Ming,[2,8,9,11] and Han-Chiao Isaac Chen[1,7,8,13,*]

[1]Department of Neurosurgery, Perelman School of Medicine, University of Pennsylvania, Philadelphia, PA 19104, USA
[2]Department of Neuroscience, Perelman School of Medicine, University of Pennsylvania, Philadelphia, PA 19104, USA
[3]Drexel University College of Medicine, Philadelphia, PA 19129, USA
[4]NMPA Key Laboratory for Research and Evaluation of Viral Vector Technology in Cell and Gene Therapy Medicinal Products, Brain Cognition and Brain Disease Institute (BCBDI), Shenzhen Institute of Advanced Technology, Chinese Academy of Sciences, Shenzhen 518055, China
[5]Center for Excellence in Brain Science and Intelligence Technology, Chinese Academy of Sciences, Shanghai 200031, China
[6]Department of Biostatistics, Epidemiology, and Informatics, Perelman School of Medicine, University of Pennsylvania, Philadelphia, PA 19104, USA
[7]Corporal Michael J. Crescenz Veterans Affairs Medical Center, Philadelphia, PA 19104, USA
[8]Institute for Regenerative Medicine, Perelman School of Medicine, University of Pennsylvania, Philadelphia, PA 19104, USA
[9]Department of Cell and Developmental Biology, Perelman School of Medicine, University of Pennsylvania, Philadelphia, PA 19104, USA
[10]The Epigenetics Institute, Perelman School of Medicine, University of Pennsylvania, Philadelphia, PA 19104, USA
[11]Department of Psychiatry, Perelman School of Medicine, University of Pennsylvania, Philadelphia, PA 19104, USA
[12]Shenzhen-Hong Kong Institute of Brain Science-Shenzhen Fundamental Research Institutions, Shenzhen 518055, China
[13]Lead contact
*Correspondence: isaac.chen@pennmedicine.upenn.edu
https://doi.org/10.1016/j.stem.2023.01.004

SUMMARY

Brain organoids created from human pluripotent stem cells represent a promising approach for brain repair. They acquire many structural features of the brain and raise the possibility of patient-matched repair. Whether these entities can integrate with host brain networks in the context of the injured adult mammalian brain is not well established. Here, we provide structural and functional evidence that human brain organoids successfully integrate with the adult rat visual system after transplantation into large injury cavities in the visual cortex. Virus-based trans-synaptic tracing reveals a polysynaptic pathway between organoid neurons and the host retina and reciprocal connectivity between the graft and other regions of the visual system. Visual stimulation of host animals elicits responses in organoid neurons, including orientation selectivity. These results demonstrate the ability of human brain organoids to adopt sophisticated function after insertion into large injury cavities, suggesting a translational strategy to restore function after cortical damage.

INTRODUCTION

Long-term neurological disability is commonly seen after traumatic brain injury,[1] stroke,[2] and other injuries to the cerebral cortex. The high burden of damage to the brain is due in large part to its limited repair capacity. While neurogenesis[3] and axon regeneration[4] occur in the adult mammalian brain, these processes are region restricted or limited and not robust enough to restore sufficient function in afflicted patients, particularly when large areas of the cortex are lost. Thus, there is a critical need to develop novel therapies for repairing cortical injuries.

Cell transplantation for the purpose of reconstructing cerebral circuitry remains one of the most promising approaches for restoring brain function. Rodent fetal cortex inserted into the cortex of adult rodents exhibit neuronal survival with extensive neurite outgrowth.[5–7] These grafts integrate locally with the brain,[6] and they appear to adopt brain network features after transplantation into the rodent visual cortex such as retinotopic maps and receptive fields.[8] These results highlight the potential of using structured neural tissues to rebuild cortex. However, fetal cortical grafts have not gained traction as a viable translational option given the ethical concerns associated with procuring this tissue in humans.

Brain organoids generated via the self-organizing properties of the progeny of human pluripotent stem cells raise the possibility that cortical repair could be achieved with autologous or

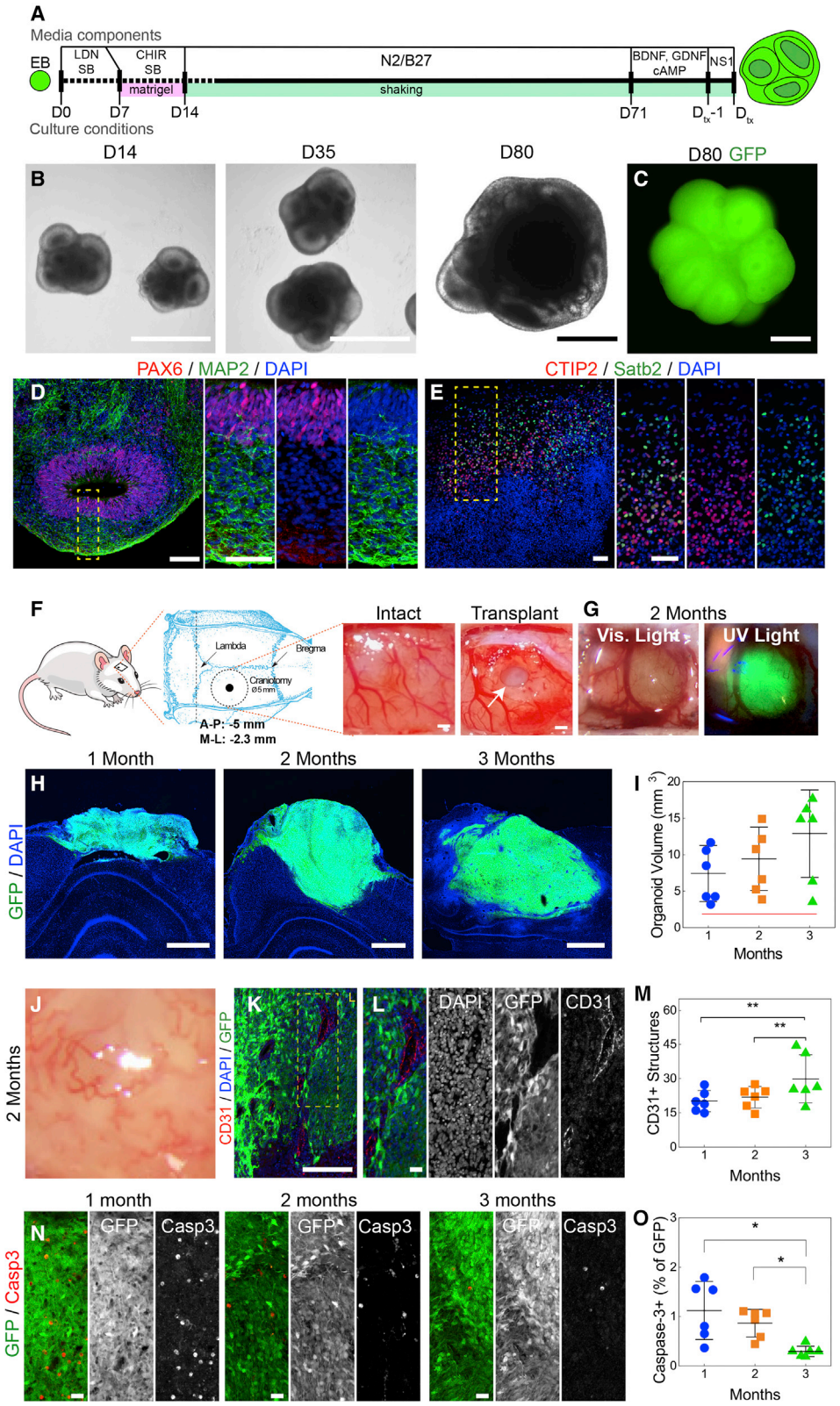

Figure 1. Human cortical organoids exhibit robust survival after transplantation into the injured visual cortex of adult rats

(A) Schematic illustrating the protocol used to generate cortical organoids (see STAR Methods for additional details). NS1, necrostatin-1; D_{tx}, day of transplantation.

(legend continued on next page)

patient-matched neural tissues, a potentially translatable version of fetal cortical grafts.[9,10] Organoids reproduce brain cell type diversity and architecture to a significant degree. Forebrain organoids develop outer radial glial cells, a distinctive feature of embryonic human cortex, and rudimentary laminar structure containing segregated upper- and lower-layer cortical neurons.[11–15] Astrocytes,[13,14,16] including human-specific astrocytes,[14] and oligodendrocytes[17] appear in these tissues at later time points, mirroring the timeline of normal neurodevelopment.

While current brain organoids do not fully replicate cortical architecture, they can be used investigate transplantation outcomes and guide efforts to improve organoid structure. Previous studies have shown the feasibility of transplanting human brain organoids into rodent hosts.[18–24] Organoid grafts are rapidly vascularized by host blood vessels[18–20] and send neuronal projections into the host brain with histological evidence of synapse formation.[18,21,24,25] These results demonstrate anatomic integration of organoid grafts with the host brain. Recently, it was shown that injection of organoids into the intact early postnatal mouse brain led to significant functional integration with the somatosensory cortex.[26] Less is known about the functional aspects of organoid graft integration with the injured adult mammalian brain. Optogenetic stimulation of organoid grafts induces local field potential (LFP) responses in the immediately adjacent host brain,[18] and visual stimulation of host animals evokes simple LFP and multi-unit activity responses in the grafts.[25] More sophisticated investigations of the functional integration of organoid grafts with systems-level networks in the context of the injured adult brain, which holds significance from a translational perspective, are needed, especially at the level of individual neurons.

Here, we sought to develop a deeper understanding of the integration of human cortical organoids with the adult rat visual cortex after transplantation into a large cortical injury. In addition to standard histological analysis of organoid grafts, we characterized the quantity and distribution of graft efferents and afferents, the latter using virus-based trans-synaptic tracing. The spontaneous activity of single units within organoid grafts was analyzed using high-density laminar multi-electrode probes. Taking advantage of the multiple tiers of neural activity present in the visual cortex, we evaluated evoked activity in response to different forms of visual stimulation of the host animal to determine the degree to which the graft had integrated with the host's visual system. Organoid grafts survived robustly after transplantation with evidence of both efferent and afferent connectivity with the host brain in primarily a visual network-specific manner. We unequivocally showed the presence of a polysynaptic pathway between the retina of host animals and organoid grafts. Neurons within organoid grafts exhibited spontaneous activity, and a subset of these neurons responded to visual stimulation and were orientation selective. These results illustrate the degree to which cortical organoids can integrate with host brain networks after insertion into extensive injury cavities, on par with outcomes obtained from transplantation studies of dissociated neurons[27,28] and organoids[26] in the context of preserved cortical architecture. Moreover, they suggest ways to optimize the strategy of utilizing stem cell-derived neural tissues for cortical repair.

RESULTS

Long-term organoid survival after transplantation into the injured adult rat visual cortex

Forebrain cortical organoids were generated from human pluripotent stem cell lines constitutively expressing green fluorescent protein (GFP) using a previously published protocol based on dual SMAD inhibition (Figure 1A).[13] Multiple cortical units with developing neuroepithelium could be identified early with increasing cellular density at later time points (Figures 1B and 1C). Within the cortical units, concentric layers of neural progenitors (Pax6$^+$) and differentiated neurons (MAP2$^+$) surrounded a central lumen (Figure 1D). Rudimentary cortical layers could be discerned at day 80 (d80; Figure 1E).[13]

Organoids were transplanted into the visual cortex of young adult male Long Evans rats immediately after the creation of an aspiration cavity encompassing the full thickness of the cortex (Figure 1F; see STAR Methods for more details). Daily injections of cyclosporine A were used for immunosuppression in this xenograft model. Grafts were inserted at the border of primary and secondary visual cortex (centered at anterior-posterior: 5 mm posterior to bregma, medial-lateral: 2.5 mm) to avoid extensive injury to thalamocortical afferents carrying visual information from the lateral geniculate nucleus. Organoids were d80–d88 at

(B and C) Brightfield (B) and fluorescence (C) micrographs of whole organoids at different times points *in vitro* demonstrate the presence and growth of multiple cortical units.
(D) Immunofluorescence staining of sectioned organoids *in vitro* show cortical units consisting of a central lumen surrounded by layers of neural progenitors (Pax6$^+$) and differentiated neurons (MAP2$^+$).
(E) Markers for upper-layer (Satb2) and lower-layer (CTIP2) cortical neurons show the formation of rudimentary laminar structure.
(F) Schematic of the transplantation paradigm, including the location of the 5-mm craniotomy. The micrographs on the right show the appearance of the intact brain and brain after an organoid has been inserted into an aspiration cavity (arrow).
(G) Brightfield images of the same animal 2 mpt under visible (left) and ultraviolet light (right) show the integrated organoid with intact surrounding brain tissue and vasculature. The graft can be clearly identified by its GFP signal.
(H) Coronal sections of animal brains 1, 2, and 3 mpt demonstrate organoid growth over time. Composites of individual images are stitched together.
(I). Quantification of the organoid volumes over time. The red line at the bottom of the graph represents the average organoid volume at the time of transplantation.
(J–L) Brightfield (J) and fluorescence (K and L) images depict blood vessel growth (CD31$^+$) within the transplanted organoid that is most likely of host origin (GFP$^-$).
(M) The number of distinct CD31$^+$ vascular structures in the entire cross-section of an organoid is quantified.
(N) Representative fluorescent images depict the temporal progression of apoptotic cells (cleaved caspase-3$^+$) within organoid grafts.
(O) The percentage of cleaved caspase-3$^+$ cells within organoid grafts is quantified.
In (I), (M), and (O), n = 6 animals, with long horizontal bars representing means and short horizontal bars representing 1 SD. *$p < 0.05$, **$p < 0.001$ (Kruskal-Wallis test). Scale bars, 500 μm (B and C), 100 μm (D, E, K), 1 mm (F–H), and 20 μm (L and N).

the time of transplantation, older than most prior studies,[18-22,24] to allow for greater differentiation and maturation of the differentiated neurons and more segregation of upper- and lower-layer cortical neurons.

We observed robust graft survival at 1, 2, and 3 months post transplantation (mpt) with an overall graft survival rate of 82.1% with the C1.2-GFP induced pluripotent stem (iPS) cell line (Figures S1A–S1E).[13] The gross appearance of the grafts often resembled the surrounding brain with infiltration of host blood vessels into the organoid (Figure 1G). Unequivocal identification of the grafts was facilitated by their fluorescence upon exposure to ultraviolet light. Graft volumes increased over time for organoids derived from the C1.2-GFP line, although this finding did not reach statistical significance (Figures 1H and 1I). Histological analysis of the grafts demonstrated blood vessels scattered through the organoid that originated from the host brain ($CD31^+/GFP^-$; Figures 1J–1L). The numbers of these vascular structures were well established at 1 mpt and increased thereafter (Figure 1M). Examination of cleaved caspase-3 immunostaining within the graft demonstrated a decrease in apoptotic cells with time (Figure 1N and 1O). These results established that d80–d88 forebrain organoids formed healthy and well-vascularized grafts with stable sizes up to 3 mpt. Of note, grafts derived from the transplantation of intact organoids exhibited far greater survival and graft volumes compared to grafts of cells dissociated from organoids (Figures S1F–S1H).

We then evaluated the response of the host cortex to the organoid graft by histology. The astrocytic and inflammatory response in a 200-μm band of brain adjacent to the graft-host border was compared to the contralateral hemisphere as an internal control as well as an injury-only animal cohort (Figure S2A–S2L). $GFAP^+$ cells consistent with astrocytes were more prevalent in the host brain near the organoid graft at 1 mpt than at later time points (Figures S2B and S2C). Although the density of astrocytes did not quite decrease to the baseline levels seen in the contralateral hemisphere, they remained scattered throughout the brain as opposed to coalescing into a scar-like structure. Moreover, the density of astrocytes in the adjacent host brain was lower in the presence of an organoid graft compared to the injury-only condition at 2 mpt (Figures S2D and S2E). We also observed that the density of $Iba1^+$ microglia in the host brain adjacent to the graft decreased with time with no differences between the graft and injury-only groups (Figures S2F–S2I). The number of $CD68^+$ activated microglia stayed relatively stable over time with a slightly greater number of cells in the graft versus injury-only groups (Figures S2J–S2M). Within the organoid itself, the number of $Iba1^+$ and $CD68^+$ inflammatory cells did not change in a statistically significant manner over time (Figures S2O–S2U), while the number of $CD3^+$ lymphocytes was very low (Figures S2V and S2W). Thus, while transplanted organoids were not walled off from the host brain by astrogliosis and induced at most a mild microglial response in the brain, there was evidence of ongoing inflammation within organoid grafts, perhaps due to the waning effect of cyclosporine A suppression of the host immune response as previously reported.[29]

An assessment of the integrity of organoid grafts derived from the H9-GFP human embryonic stem (hES) cell line and a second iPS cell line (AICS) yielded mostly similar results with some line-specific differences. We found that host animal and graft survival rates were similar with the H9-GFP and AICS lines (Figure S1). While the H9-GFP organoid grafts were similar in size compared to the C1.2 grafts, the AICS grafts were significantly smaller and contained fewer $CD31^+$ structures at 2 mpt (Figures S3A–S3F). No significant differences were noted across cell lines in terms of apoptosis (Figures S3G–S3I). H9-GFP grafts were associated with a slightly higher number of $GFAP^+$ astrocytes in the adjacent host brain, a finding that did not reach statistical significance (H9-GFP versus AICS: $p = 0.53$, H9-GFP versus C1.2-GFP: $p = 0.052$; Figures S3J–S3L) while there was no significant difference in the number of $Iba1^+$ microglia in the host brain next to grafts derived from different lines (Figures S3M–S3O). These results indicate that organoids generated from different pluripotent stem cell lines can be viable intracerebral grafts but may be associated with line-specific differences in transplantation outcomes. To simplify analysis, subsequent experiments were limited to the C1.2-GFP line.

Cellular composition of organoid grafts

To characterize how the cellular composition of the organoid grafts evolved over time, we performed histological analyses of the progenitor, neuronal, and glial compartments of the grafts. Organoid grafts were confirmed to be of human origin with STEM121 immunostaining (Figures 2A and 2B). Abundant $Pax6^+$ and fewer $Sox2^+$ neural progenitors were found in the grafts (Figures 2C–2E). As would be expected of a maturing graft, the number of $Pax6^+$ neural progenitors decreased from 1 to 3 mpt, although a significant pool of progenitors remained at 3 mpt as a percentage of all GFP^+ cells (Figure 2D). We did not find any evidence of $Oct4^+$ pluripotent cells in the graft (Figures S4G and S4H).

More mature neurons were identified throughout the graft (Figures 2F and 2G), with the number of $NeuN^+$ neurons increasing over time (Figure 2H). The overwhelming majority of the cells within the graft expressed FoxG1, indicative of their telencephalic nature (Figure 2I). Few cells expressed Sp8, while many were positive for Coup-TF1 (Figures S4A–S4C), suggestive of an occipital cortex phenotype that has been seen with both dissociated cortical neurons[29] and forebrain organoids[11] derived from dual SMAD inhibition protocols. Both excitatory and inhibitory neurons were found in the organoid grafts (Figures S4D–S4F). The ratio of excitatory to inhibitory neurons was 4.3:1, 3.3:1, and 3.7:1 at 1, 2, and 3 mpt, respectively, in line with the roughly 4:1 ratio typically found in the normal adult human cortex. We did not find any evidence of host neurons migrating into the organoid grafts (Figures S4K and S4L).

Given the importance of laminar architecture in cortical processing[30–32] and the presence of rudimentary cortical layers in the organoids before transplantation (Figure 1E),[13] we were interested in determining the degree of cortical structure that was present *in vivo*. Cells expressing transcription factors associated with cortical layers II/III (Cux1, Satb2), IV (Necab1), and V/VII (CTIP2, Tbr1) could all be identified in the organoid grafts (Figures 2J–2N). There was some overlap between $Pax6^+$ and $Tbr1^+$ cells (1 mpt: 7.25% ± 2.26%, 2 mpt: 8.37% ± 3.36%, 3 mpt: 5.04% ± 3.04%; mean ± SD n = 6 animals), which has previously been reported in the developing human brain.[33] The number of $CTIP2^+$, $Cux1^+$, and $Satb2^+$ cells increased over

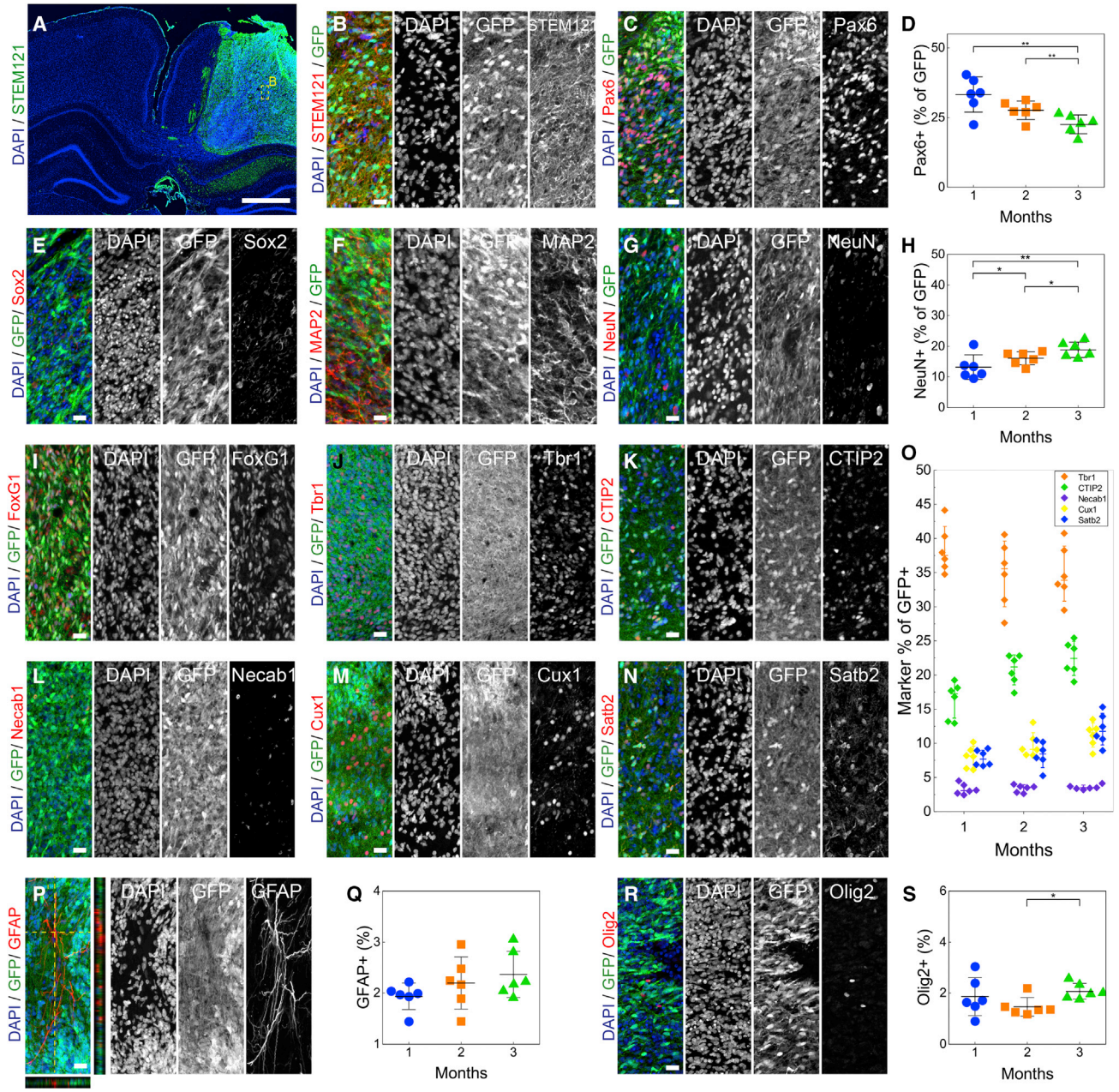

Figure 2. Organoid grafts demonstrate progressive cellular maturation

A broad panel of immunohistochemical markers was imaged with confocal microscopy to evaluate the cellular composition of the organoid grafts. Fluorescent micrographs in this figure are all at 2 mpt.

(A) This low-magnification micrograph (composite of individual images that are stitched together) depicting STEM121 staining shows the location of the high-magnification images in (B). The other high-magnification micrographs in this figure are similar in location to (B).

(B) STEM121 confirms the human origin of the vast majority of the graft cells (GFP^+).

(C and E) Neural progenitors are identified with Pax6 (C) and Sox2 (E).

(D) Quantification of $Pax6^+$ cells shows a decline in this population over time.

(F and G) The presence of differentiated neurons is shown using MAP2 (F) and NeuN (G).

(H) Quantification of NeuN demonstrates an increase in the number of mature neurons in the organoid graft over time.

(I) The majority of graft cells are positive for FoxG1, a telencephalic maker.

(J–N), Cells in the organoid graft express markers for cortical layers V (Tbr1, CTIP2), IV (Necab1), and II/III (Cux1, Satb2).

(O) Quantification of these cortical layer markers demonstrates increasing $CTIP^+$, $Cux1^+$, and $Satb2^+$ cells and decreasing $Tbr1^+$ cells over time.

(P and Q) Astrocytes are identified with GFAP (P), which is quantified in (Q) Reconstructions of confocal z stacks show no co-localization of GFAP with GFP.

(R and S) Oligodendrocytes are identified with Olig2 (R), which is quantified in (S).

In (D), (H), (O), (Q), and (S), n = 6 animals, with long horizontal bars representing means and short horizontal bars representing 1 SD*$p < 0.05$, **$p < 0.001$ (Kruskal-Wallis test). Scale bars, 1 mm (A), 20 μm in all other micrograph panels.

time (Figure 2O). However, we did not observe distinct architecture in the organoid grafts, including the cortical layers seen *in vitro*. Thus, while cortical neurons in the organoid grafts appeared to mature over time, there was a loss of neuronal layer structure in the organoids after transplantation. The possibility that vertical connectivity (i.e., thalamus→layer IV→layer II/III→layer V→layer VI→thalamus) persists in the absence of laminar structure remains to be investigated.

Glial cells are integral parts of functioning brain circuitry, and prior studies have demonstrated their presence in forebrain organoids *in vitro*.[13,16] GFAP$^+$ cells consistent with astrocytes were scattered throughout the organoid grafts (Figures 2P and 2Q). These cells were low in number compared with the ratio of astrocytes to neurons found in the normal human brain.[34] We also found that the organoid grafts contained small numbers of Olig2$^+$ oligodendrocytes (Figures 2R and 2S). The majority of both astrocytes and oligodendrocytes in the graft were STEM121$^-$ and thus originated from the host (Figures S4M–S4P). Previous studies have shown that longer periods of time are needed for these cell types to develop in cortical organoids.[13,17] Thus, organoid grafts contain a complement of glial cells primarily derived from the host brain that could support neuronal function, although the number of these cells is lower than the normal brain.[35]

Graft efferents project to visual system targets

Functional integration of transplanted organoids with the host brain depends upon the formation of appropriate connections between graft neurons and host brain circuits. We first investigated the extent of efferent graft projections into the host brain, as well as their anatomical targets. Prior transplantation studies reported that the connectivity patterns of graft neurons depend heavily on their stage of development, which dictates whether connections are formed based on the intrinsic phenotype of the grafted cells or the identity of the host transplantation site.[36,37] Because the organoid grafts exhibited primarily an occipital identity and were transplanted homotopically into the visual cortex, we hypothesized that the majority of their axon projections would target parts of the visual system.

As has been reported for neuronal grafts derived from dissociated cells in the cerebral cortex,[27,37] the greatest abundance of graft projections was found in the cortex directly adjacent to the graft (Figures 3A–3C). We noted that the GFP border of the graft was hazy in some areas because of extensive projections into the host brain (Figure 3B) while it was quite distinct in other areas (Figure 3D). We also observed graft efferents in more distant cortex in the ipsilateral hemisphere, up to 1.85 mm from the graft (Figures 3D–3G). Although no projections were observed in the contralateral cortex, they did appear in the corpus callosum crossing the midline (Figures 3H and 3I). Projections were also found in subcortical structures such as the thalamus (Figure 3J). In 4 of 6 animals, thalamic projections were observed in nuclei associated with the visual and limbic circuits, particularly lateral geniculate (LG) and lateral posterior (LP) (Figure 3O). Fewer projections were found in the sensorimotor and auditory nuclei of the thalamus. These nuclei were identified by overlaying rat atlas maps over histological images. Co-labeling with tau and NF200 and the absence of MAP2 confirmed that these graft projections were axonal in nature (Figures 3K and 3L). Minimal myelin basic protein was found around the projections, indicating the lack of myelination (Figures 3L). The presence of human synapsin protein at the interface between graft projections and the host brain suggested the formation of putative synapses between the graft and host brain (Figure 3M).

While the density of graft projections increased in some regions of the host brain from 1 to 3 mpt, the efferent targets themselves did not change appreciably (Figure 3N). Most of the projections were found in the visual and retrosplenial cortex, and their density, as determined by GFP$^+$ area, increased over time. The density of projections also increased in the motor cortex, corpus callosum, and hippocampus, while they stayed relatively stable in the somatosensory/parietal cortex and thalamus. On the whole, the targets of these efferents were primarily part of the visual system, similar to what has been observed with other neural transplantation studies.[27,37,38] However, we did not see graft projections in the striatum or superior colliculus, which was reported in these other studies. We also observed some off-target projections as well, especially in the motor cortex and motor nuclei of the thalamus (Figure S5).

Graft afferents originate from visual system sources

While graft efferents provide insight into the anatomical connectivity of organoid grafts, appropriate inputs carrying visual information from the host brain would be the direct mediators of the functional integration of graft neurons with the host visual network. Thus, we mapped the source of graft afferents from the host brain at 2 mpt using two virus-mediated trans-synaptic tracing strategies. First, we employed the modified rabies virus (RABV) system for monosynaptic retrograde tracing (Figure 4A).[27,39] Organoids for this study were derived from the C1.2 iPS cell line that had been modified to constitutively express the RABV tracing mechanism (DsRed-G-TVA800). Organoid grafts showed abundant dsRed signal, demonstrating continued expression of the RABV tracing mechanism *in vivo* (Figures 4B–4D). As with graft efferents, the greatest number of graft afferents originated from the visual cortex immediately adjacent to the graft (Figures 4E–4G and 4S). Additional GFP$^+$ afferents could be seen in more remote cortical regions in the ipsilateral hemisphere (Figures 4H and 4I), bilateral hippocampi (Figures 4J–4O), and thalamus (Figures 4P–4R). Within the thalamus, the lateral geniculate nucleus provided more afferents to the organoid graft than other thalamic nuclei except for LP, which is also known to provide inputs to the occipital cortex, and ventrolateral (VL), a motor nucleus (Figure 4T). These afferent sources indicated appropriate connectivity between the organoid graft and the host visual network, but they also revealed non-visual inputs. Some non-visual thalamic afferents are present in the visual cortex itself.[27] However, it is also possible that the organoid grafts exhibit incomplete pruning, perhaps due to insufficient organoid activation during normal visual function or the limited duration of our analysis. Parsing through these possibilities will require additional investigation using long-term longitudinal studies of organoid grafts with greater degrees of circuit maturation.

To evaluate connectivity between the organoid graft and further upstream sources of visual information, particularly the retina, we used the modified herpes simplex virus (HSV) system for polysynaptic anterograde tracing (Figure 5A).[40]

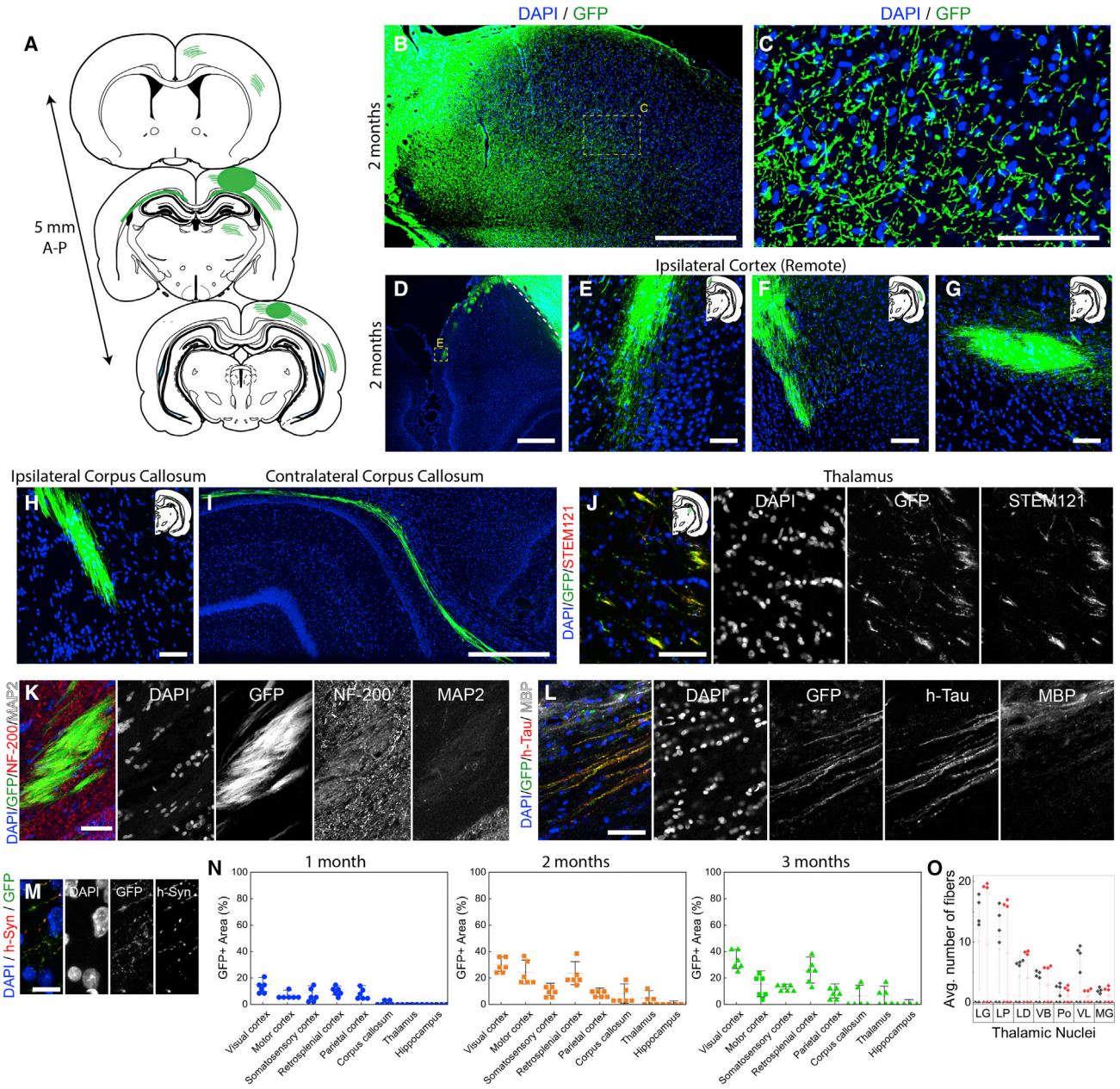

Figure 3. Transplanted organoids send projections widely into the host brain

(A) This schematic illustrates the approximate location of projections from the organoid graft 2 mpt.

(B and C) Low- (B) and high- (C) magnification views of the host cortex adjacent to the transplanted organoid on a coronal section show a high-density of GFP$^+$ projections adjacent to the graft. (B) is a composite of individual images that are stitched together.

(D–G) More remote GFP$^+$ projections are found in the retrosplenial cortex medial to the graft (D and E), auditory cortex laterally (F), and visual cortex lateral to the graft (G). The dotted line in the upper right corner of (D) defines the border between the organoid graft and host brain. (I) is a composite of individual images that are stitched together.

(H–J) Graft projections are also identified in the ipsilateral (H) and contralateral (I) corpus callosum, as well as the thalamus (J). GFP$^+$ processes within the thalamus co-localize with STEM121, confirming their human origin. The schematics in the upper right corner of (E)–(H) and (J) show the location of the GFP$^+$ processes in the brain for that panel. In (D)–(I), green is GFP and blue is DAPI. (K) GFP$^+$ processes co-localize with NF-200 (red), but not MAP2, a somatic and dendritic marker (white).

(L) These processes also co-localize with tau (red), an axonal marker. These processes do not appear to be myelinated (myelin basic protein, white).

(M) GFP$^+$ processes in the host brain also co-localize with human synapsin (red).

(N) The number of GFP$^+$ projections is quantified in different regions of the brain at 1–3 mpt.

(O) The number of GFP$^+$ projections is quantified in different thalamic nuclei at 2 and 3 mpt.

In (N) and (O), n = 6 animals, with long horizontal bars representing means and short horizontal bars representing 1 SD. Scale bars, 500 μm (B, D, and I), 100 μm (C and F), 50 μm (E, G, H, J, K, and L), and 10 μm (M).

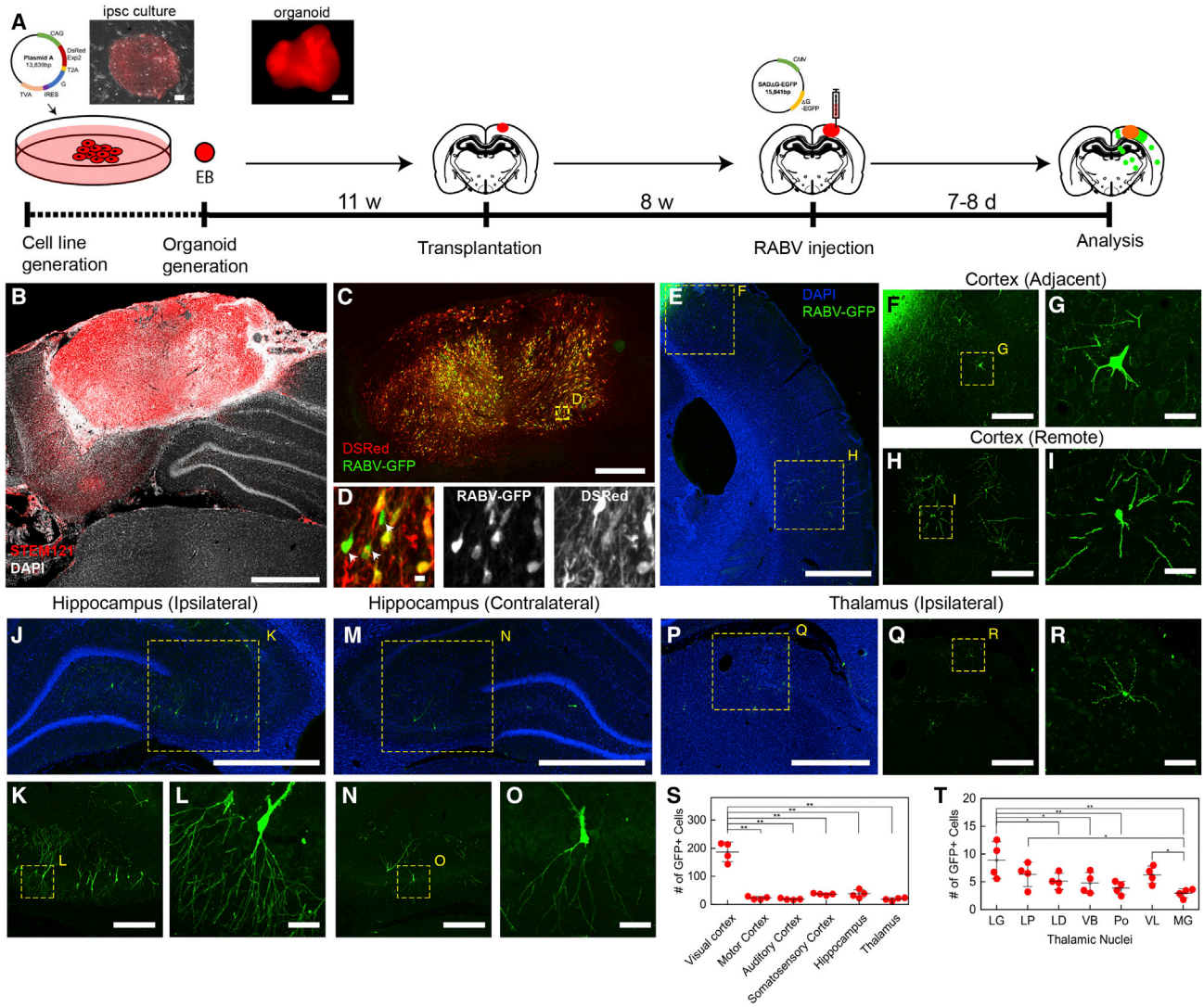

Figure 4. Organoid grafts receive afferent inputs from multiple regions of the rodent brain

(A) This schematic illustrates the timeline for using the modified rabies system for monosynaptic retrograde tracing to analyze organoid graft afferents.

(B) Transplanted organoids were immunostained with STEM121 (red) to confirm the human origin of the graft.

(C and D) Uninfected cells within the organoid express dsRed^{+} alone. Organoid cells infected by RABV-GFP express both dsRed and GFP and are thus yellow. Cells that only express GFP (arrows in the right panel of D) are trans-synaptic partners that are upstream of the yellow "starter" cells. All GFP^{+} cells in the organoid co-localize with STEM121 and are thus of human origin (see Figure S6).

(E–R) Regions of the host brain providing monosynaptic input to the organoid graft include adjacent visual cortex (F and G), more remote somatosensory cortex (H and I), ipsilateral (J–L) and contralateral hippocampi (M−O), and the ipsilateral thalamus (P–R). (B), (C), (E), (J), (M), and (P) are composites of individual images that are stitched together.

(S and T) The number of GFP^{+} cells that are monosynaptically connected with organoid grafts is quantified by brain region (S) and thalamic nuclei (T). In (S) and (T), n = 4 animals, with long horizontal bars representing means and short horizontal bars representing 1 SD. *$p < 0.05$, **$p < 0.001$ (Kruskal-Wallis test). Scale bars, 1 mm (E, J, M, and P), 500 μm (B and C), 300μm (F, H, K, N, and Q), 50 μm (G, I, L, O, and R), and 10 μm (D).

Two months after transplanting non-fluorescent organoids, HSV-GFP was injected in the host animal's eye contralateral to the side of the organoid graft. One week after HSV injection, abundant GFP^{+} cells were present in the organoid graft and co-localized with the STEM121^{+} (Figures 5C and 5D). These GFP^{+} cells also co-labeled with the neuronal marker βIII-tubulin, but not GFAP (Figures 55E and 5F). As expected, GFP^{+} cells were found in the host visual cortex adjacent to the graft (Figure 5G), as well as the ipsilateral lateral geniculate nucleus (Figures 5H and 5I), and optic nerve contralateral to the organoid graft (Figures 5J and 5K). Interestingly, the density of GFP^{+} cells in the organoid was 2.75 times greater than in the naive visual cortex and 3.94 times greater than adjacent host visual cortex (Figures 5L–5N), perhaps the result of an over-abundance of connectivity within the organoid before pruning of connections has occurred. These data unequivocally demonstrate that retinal output reaches the organoid graft via synaptic connections.

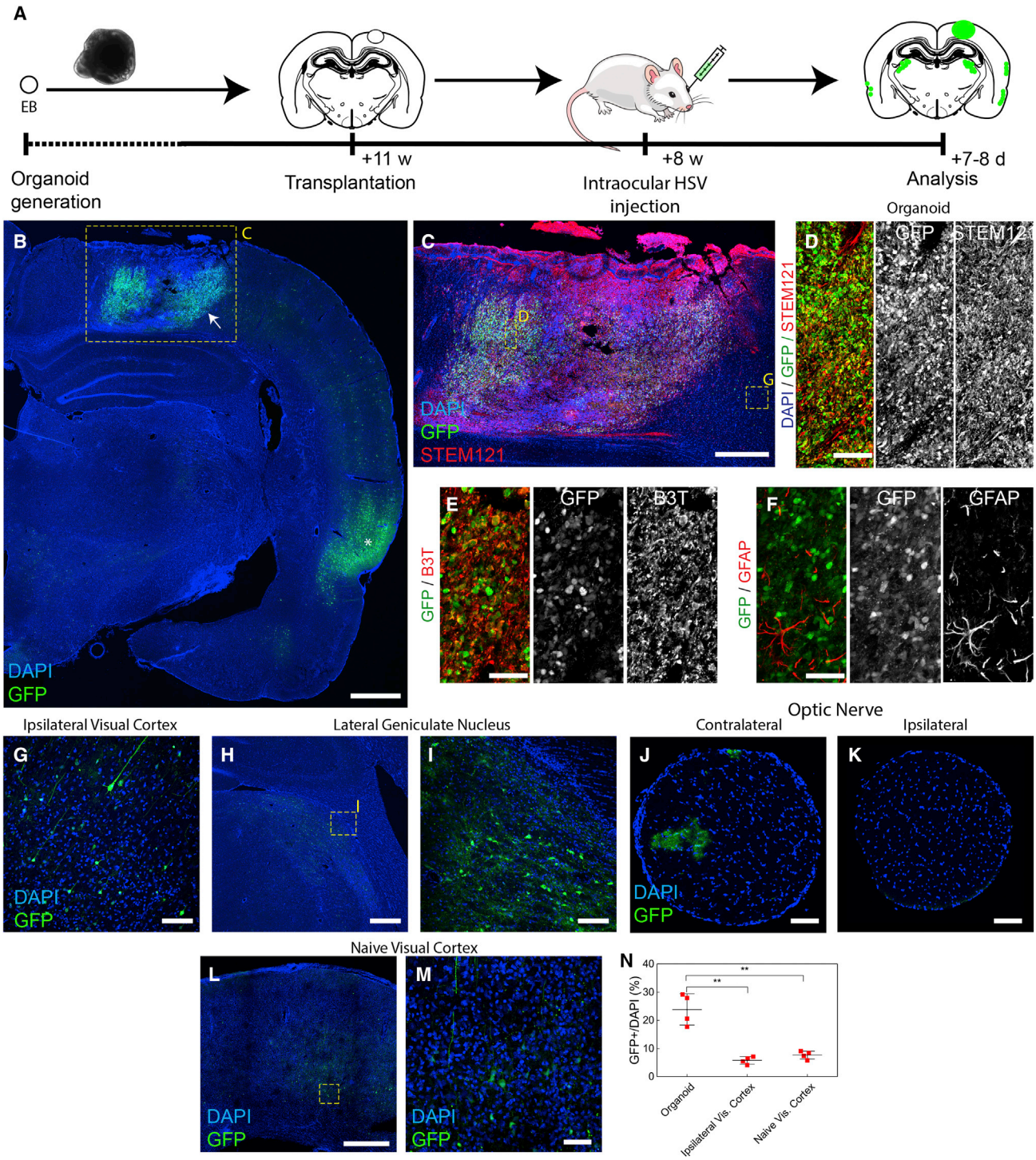

Figure 5. A polysynaptic pathway exists between the retina of the host animal and transplanted organoids

(A) This schematic shows the timeline for using modified HSV for polysynaptic anterograde tracing.

(B) A low-magnification micrograph of the right hemisphere of the brain (coronal section) shows GFP$^+$ cells within the organoid (white arrow) and multiple regions of the host brain. The densest area of GFP$^+$ cells in the host brain corresponded to the entorhinal cortex (asterisk).

(C) A human antigen marker (STEM121, red) was used to identify the non-fluorescent graft.

(D) A high-magnification view of the organoid shows a high density of GFP$^+$ cells co-localizing with STEM121.

(E) HSV-labeled cells (GFP$^+$, green) within organoid grafts are neuronal in nature, as evidenced by co-labeling with the neuronal marker βIII-tubulin (red).

(F) In contrast, these HSV-labeled cells (GFP$^+$ green) do not co-localize with GFAP (red) and are thus unlikely to be astrocytes.

(legend continued on next page)

Organoid grafts exhibit robust spontaneous neural activity

Having documented extensive efferent and afferent connectivity between organoid grafts and the host brain by histology, we next evaluated the functionality of the grafts using *in vivo* extracellular recordings. Laminar silicon probes with 32 electrode contacts were inserted into organoid grafts using their intrinsic fluorescence under ultraviolet light for visual guidance (Figure 1G). Electrode tracks were identified histologically post hoc, and any electrophysiological data that was determined to be within 100 μm of the host-graft border were discarded to minimize signal contamination by surrounding normal brain activity (Figures S7A–S7D), similar to a previously described methodology[41]

We recorded from a total of 10 animals that had been transplanted with organoids derived from the C1.2-GFP line and 2 naive rats. All 10 organoid grafts demonstrated spontaneous neural activity (n = 1 at 1 mpt, 6 at 2 mpt, and 3 at 3 mpt) as did both naive animals. Biphasic spike waveforms were identified in both transplanted organoids and the visual cortex of naive animals (Figures 6A, 6B, S7F, and S7G). After excluding units within 100 μm of the graft-host border, we found that units were distributed throughout the depth of the organoid (mean: 830 μm from the graft-host border, range 100–1,780 μm; Figures S7H–S7K).

Spontaneous units within the organoid were substantially similar to neurons in the naive rat visual cortex and demonstrated stability of unit parameters over time after transplantation (Figures S7L–S7O). No significant differences between organoid and rat cortex neurons were found in firing rates ($p = 0.562$), spike amplitude ($p = 0.155$), or spike width ($p = 0.973$) (Table S1). There was also no significant effect of post-transplantation time point on any of these parameters in organoid units (firing rate: $p = 0.470$, spike amplitude: $p = 0.670$, spike width: $p = 0.370$). Normalized depth of the unit had a significant effect on firing rate with greater proximity to the graft-host border associated with higher firing rates ($p = 0.015$), perhaps reflecting the greater degree of host inputs near this interface.

To confirm the physiological nature of the spontaneous organoid units, we transplanted two additional animals with organoids generated from the H9-hM4Di ES cell line, which encodes a designer receptor exclusively activated by a designer drug (DREADD) that diminishes neural activity in the presence of clozapine N-oxide (CNO). At 2 mpt, spontaneous neural activity was recorded from the organoid graft and adjacent brain before and after administration of CNO (3 mg/kg). While no change in the neural activity of the brain was noted, a significant decrease in activity was observed in the organoid graft in response to CNO administration (Figures S7S–S7U). This result demonstrated functional integration of brain organoids from different pluripotent stem cell lines and confirmed the electrical nature of the recorded activity.

Organoid neurons integrate functionally with the host visual network

A previous study established that organoid grafts can integrate with the host brain at the local circuit level[18] However, more sophisticated integration, especially at a system level, would be necessary for organoid grafts to contribute to the recovery of brain function after injury. We thus examined how neural activity in organoid grafts responded to visual stimulation of the anesthetized host animal.

We initially provided visual stimulation to 8 of the 10 transplanted animals (n = 1 at 1 mpt, 5 at 2 mpt, and 2 at 3 mpt) and both naive animals using a simple screen on-screen off paradigm (50-ms pulse width, 0.5 Hz). Visually evoked neural activity was detected for 6 of the 8 transplanted (0/1 at 1 mpt, 4/5 at 2 mpt, and 2/2 at 3 mpt) and both naive animals. None of the 7 cells that were active spontaneously in the 1 mpt organoid graft exhibited evidence of evoked activity. However, at 2 mpt, 31/140 cells (22.1%) were evoked and 10/140 cells (7.1%) were suppressed by visual stimulation across 5 animals. At 3 mpt, 7/33 (21.2%) cells were evoked by visual stimulation, and no cells were suppressed (Figure S7P). The pattern of evoked unit activity in the organoid was qualitatively similar to that observed in naive rat visual cortex (Figures 6D–6G), suggesting that organoid neurons have a comparable potential for light responsiveness to visual cortex neurons.

Some differences between organoid and visual cortex neurons were observed. In comparison to visual cortex neurons in naive animals (Figures 6D and 6F), the response of organoid neurons to visual stimulation was more prolonged with several activation peaks (Figures 6E and 6G), perhaps as a result of the increased internal connectivity of the organoids (Figure 5N). We also observed that visual stimulation of the host animal evoked event-related potentials (ERPs) in the organoid (Figure 6G), but these ERPs were smaller in amplitude than those seen in the visual cortex of naive animals (Figure 6F). Finally, fewer graft neurons exhibited evoked activity compared to neurons in the naive visual cortex (22/30 cells, 73.3%; $p = 0.005$).

Next, eight different orientations of drifting grating stimulation were presented to a subset of host animals (n = 2 at 2 mpt and 2 at 3 mpt) to determine whether organoid graft neurons could encode for features of the visual stimulus. Particularly at 2 mpt, some graft units exhibited tuning responses that indicated the presence of orientation selectivity (Figures 6J and 6K), similar to what was observed in visual cortex neurons (Figures 6H and 6I). Interestingly, the distribution of orientation selectivity indices between organoid neurons (both 2 and 3 mpt) and naive visual

(G–K) Micrographs demonstrate the presence of GFP^+ cells in expected parts of the visual pathway, including the visual cortex adjacent to the organoid (G), lateral geniculate nucleus of the thalamus (H and I), and the optic nerve contralateral, but not ipsilateral, to the organoid graft (J and K).
(L and M) The presence of GFP^+ cells in the visual cortex of naive animals treated with retinal injections of HSV-GFP is shown. (B), (C), (H), and (L) are composites of individual images that are stitched together.
(N) Quantification of the GFP^+ cells demonstrates a significantly higher density of these cells in the organoid compared to adjacent visual cortex and visual cortex in naive animals without organoid grafts.
In (N), n = 4 animals, with long horizontal bars representing means and short horizontal bars representing 1 SD. $^{**}p < 0.01$ (Kruskal-Wallis test). Scale bars, 1 mm (B), 500 μm (C, H, and L), 100 μm (G, I, J, K, and M), and 50 μm (D–F).

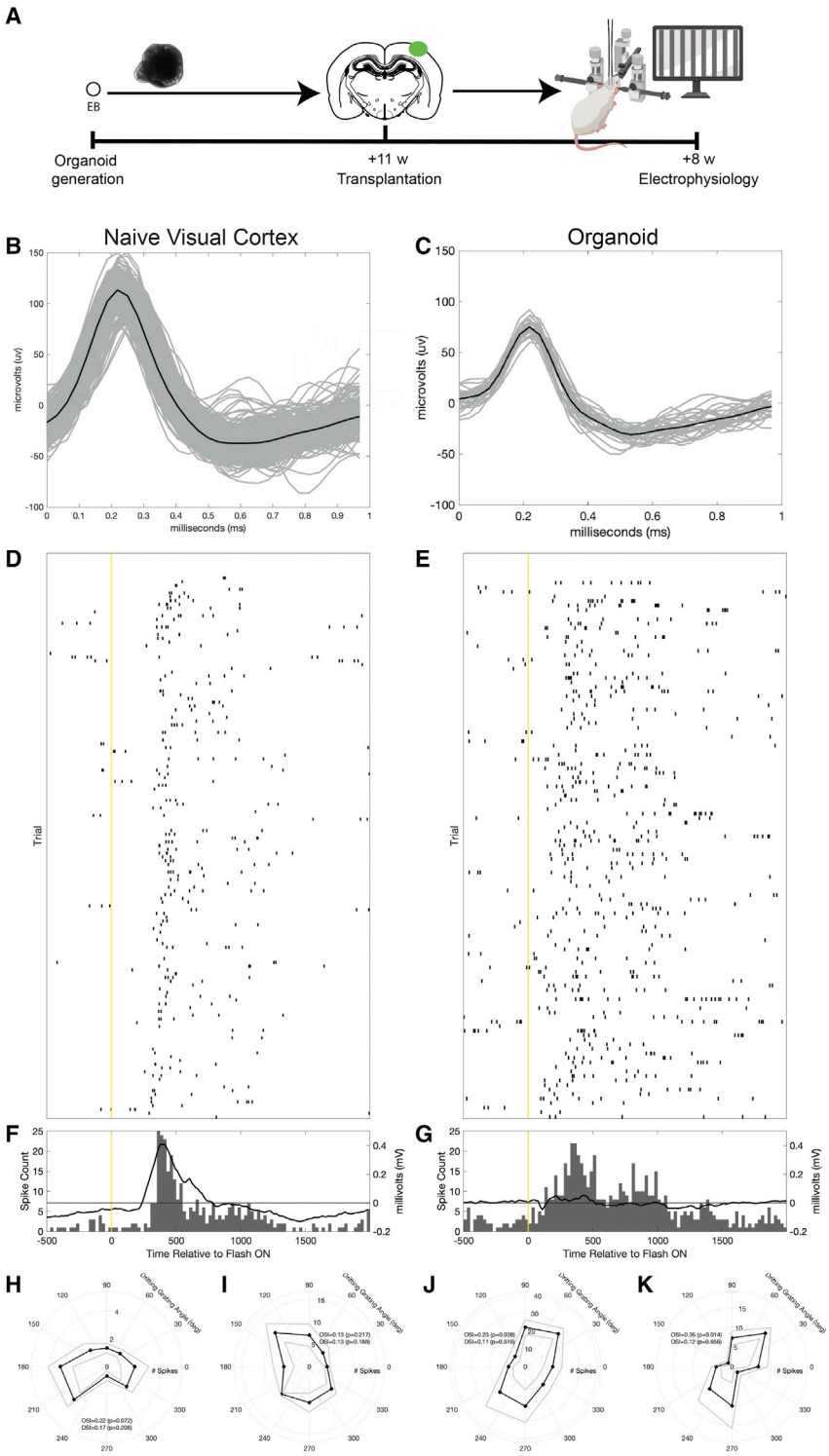

Figure 6. Transplanted organoids functionally integrate with the host visual system

Neural activity from naive visual cortex and an organoid graft at 2 mpt is shown on the left and right, respectively.

(A) Schematic of the experimental design with visual stimulation and electrophysiological recordings.

(B and C) Representative single-unit waveforms recorded from the visual cortex of animal naive-1 (B) and the organoid graft in animal 2M-1 (C) are depicted. The gray lines are single spikes, and the black line indicates the average waveform across all recorded spikes.

(D and E) Raster plots of single units recorded from naive-1 (D) and the organoid graft in 2M-1 (E) are shown across 140 and 120 trials, respectively. The yellow line corresponds to the timing of a 0.5-Hz flashing screen stimulus.

(F and G) Peri-stimulus time histograms (PSTH; gray bars, left axis) and the ERPs detected at the channel where the unit had the greatest amplitude (black line, right axis) are plotted for representative evoked units recorded from the visual cortex in naive-1 (F) and the organoid graft in 2M-1 (G). These are the same units as depicted in (D) and (E). Again, the yellow lines correspond to the 0.5 Hz flashing screen stimulus.

(H–K), Rose plots show the number of times a single unit fired based on the orientation of a presented drifting grating for two example units recorded from naive-1 (H and I) and the organoid in 2M-1 (J and K). These units show preferential firing for drifting gratings in a particular orientation. Black lines indicate the average number of spikes across trials and gray lines correspond to 1 SE above and below the mean. Angle measures around the periphery of the rose plot indicate the orientation of drifting grating presentation (degrees). The radial axis indicates the firing rate of the neuron in response to that orientation of drifting grating (Hz). OSI, orientation selectivity index.

cortex was not statistically different from each other ($p = 0.649$; Figure S7Q). These findings demonstrate that transplanted organoids are capable of integrating with the host visual system, exhibiting evoked unit and LFP activity as well as adopting feature selectivity.

DISCUSSION

Reconstructing brain circuitry after injury to restore cerebral function is a long sought-after goal of regenerative medicine. Brain organoids are intriguing candidates for brain repair substrates by virtue of their organized structure and the potential for autologous or patient-matched grafts. Here, we sought to better understand the potential of forebrain organoids to integrate with brain networks in the injured adult brain using the visual system as a platform for assessing the degree of functional graft integration.[8,25,27,28] Our findings indicate that brain organoids are capable of replacing large cortical cavities and integrating into the circuitry of systems-level networks in the brain, which supports the use of pluripotent stem cell-derived neural tissues for repair of brain circuitry.

Integration potential of different neural transplantation substrates

The vast majority of intracerebral neural transplantation studies have involved injections of dissociated cells. Recent studies employing this approach to generate cortical grafts have investigated the electrophysiological aspects of graft integration with host cortex. Insertion of rat embryonic neurons into a focal lesion in layer II/III[27] and distribution of hES cell-derived cortical neurons across an otherwise intact cortex via fetal intraventricular transplantation[28] both lead to striking degrees of systems-level integration with the visual network, including the demonstration of orientation selectivity by graft neurons. It is important to note that this sophisticated degree of functional integration was achieved in the context of relatively preserved cortical architecture. In contrast, grafts derived from dissociated mouse ES cells[38] or human iPS cells[41] that are transplanted into extensive cortical lesions develop evoked activity to sensory stimuli but not more complex responses. Similarly, human iPS cell-derived cortical neurons inserted adjacent to a stroke cavity in motor cortex adopt a non-specific role in motor function but do not contribute to the observed reversal of motor behavioral deficits.[42] These studies imply that intact cortical architecture facilitates the adoption of higher-order neural function by graft neurons and suggest the need to restore cortical structure when neural transplantation targets larger cortical lesions (Table S2).

Transplantation of pre-formed "auxiliary cortical columns" may be the ideal solution for larger cortical lesions that approximate clinical pathology. Fetal cortex is an obvious choice to fit this role. Previous studies have documented the ability of rodent fetal cortical grafts to develop sophisticated features such as receptive fields and feature selectivity in the visual cortex.[8] Nonetheless, the translation of fetal cortical grafts has been severely impaired by their associated ethical quandaries.

Human brain organoids could potentially serve as a translatable version of fetal cortical grafts by virtue of their cortical structure and stem cell origin. A recent study showed that organoids injected into the intact postnatal rat brain integrated functionally with not only the somatosensory cortex, the site of injection, but also the broader brain, as evidenced by the observation that optogenetic stimulation of the graft drove behavior on a conditioning task.[26] This model advances the use of brain organoids as models for investigating neurodevelopment and its associated disorders. Our data extend these results, showing that human organoid grafts can achieve comparable degrees of functional integration with host brain networks in the context of the injured adult mammalian brain, establishing organoid transplantation as a neural repair strategy. The comparison of outcomes between intact and dissociated organoid grafts further highlights the technical and survival advantages of neural tissues over dissociated cells for addressing extensive cortical injuries. Another recent study used chronically implanted graphene arrays to investigate electrophysiological responses of organoids inserted into aspiration cavities in adult mice, showing that visual stimulation of host animals evokes LFP and multi-unit activity responses in organoid grafts.[25] Our results corroborate and extend these findings, demonstrating that single units in organoid grafts also respond to visual stimulation of host animals. Importantly, we showed that some of these responsive single units develop orientation selectivity, a sophisticated feature unique to the visual system, and elucidated an initial roadmap of graft-host connectivity using virus-based trans-synaptic tracing. These data provide further insight into the integration potential of brain organoids with the injured adult mammalian brain.

However, the organoids used in this study fall short of the concept of auxiliary cortical columns in two respects. First, the cortical layer separation in the organoids that were used for this study was rudimentary.[13] Progress has since been made in generating a more distinct laminar structure in forebrain organoids[14] Moreover, our understanding of the microcircuitry within brain organoids and the circuit-level activity of these entities remains at an early stage.[43] Further advances in these areas, as well as better control over the number of cortical units per organoid and supplementation of interneurons,[44–46] will yield organoid grafts that better resemble the cortex. Second, preservation of organoid structure after transplantation was incomplete. Laminar structure is disrupted even in fetal cortical grafts, although some level of cortical layer organization remains.[7] A better understanding of the insults that degrade tissue architecture post transplantation is necessary to develop strategies for counteracting these insults, which could include the use of extracellular matrix components to protect organoid grafts.[47]

Factors impacting organoid graft viability

We found consistently high rates of organoid graft survival 1–3 mpt, in line with previously reported results for transplanted whole-brain[18] and forebrain organoids.[21] Accumulating evidence suggests that neural tissues possess advantages over dissociated cells with respect to transplantation outcomes. Neurons grown on polymeric scaffolds demonstrate better survival than the same neurons in suspension after transplantation.[48,49] Brain organoids exhibit similar benefits of improved neural survival and vascularization after *in vivo* engraftment compared with dissociated neural progenitors[19] Cell-cell interactions within a three-dimensional environment and the presence of an extracellular matrix likely contribute to these findings by preserving the viability of neural tissues early after transplantation.

Long-term health of transplanted organoids is a function of adequate graft perfusion and host immunosuppression. Because of the limits of diffusion, vascularization of organoids is essential for continued graft viability and growth. The presence of $CD31^{+}$/GFP^{-} structures in the organoid grafts in this study demonstrated their progressive vascularization by the host brain, which was sufficient to support organoid viability and long-term growth. Other studies have documented that organoid grafts decrease in size in the first 10–14 days after transplantation, the time period before host vasculature infiltrates the graft,[18,19] and that incorporating networks of endothelial cells within the organoid prior to transplantation promotes improved graft health.[20] Accelerating organoid vascularization in this manner could have potential benefits on more sensitive transplantation outcomes, including graft architecture and activity. Daily immunosuppression with cyclosporine A enabled xenograft survival up to 3 months with diminishing numbers of apoptotic and microglial cells surrounding the graft. However, the persistent, and perhaps increasing, presence of inflammatory cells within the graft suggest the flagging efficacy of this strategy. These results confirm the need for transplantation into genetically immunosuppressed animals for longer-term studies.[18,28,29,42]

Patterns of graft connectivity with the host brain

We observed that the organoid grafts formed connections primarily with known parts of the visual network, both from an efferent and afferent perspective. The forebrain organoids transplanted in this study showed a bias toward an occipital phenotype (i.e., more expression of COUP-TF1 than Sp8), which is commonly seen with current cortical differentiation protocols based on dual SMAD inhibition[11,50] Thus, it is not surprising that our "homotopic" transplantation paradigm resulted in mostly appropriate connections between an "occipital cortex" organoid graft and the host visual system. We chose to use d80–d88 organoids for transplantation because of the well-established presence of both upper- and lower-layer cortical neurons at these time points, which could improve the systems-level integration potential of these grafts. However, the optimal age for organoid transplantation has not yet been established, especially with regards to the balance between neuronal/circuit maturity and cellular plasticity. Younger organoid grafts (d42–d55) are associated with a greater number of proliferating cells[23] and more projections into the host brain,[21] but the impact of these factors on organoid graft integration has not been investigated. In addition, younger organoids hold the risk of overgrowth that could impair brain function.[21] Organoid age is even more important to consider for "heterotopic" transplantation strategies. Previous transplantation studies using rodent[36,51,52] and human[37] cells indicate that less mature neurons adopt the connectivity patterns of the local host environment while older neurons connect with the host brain based on their intrinsic identity. Developing a greater understanding of the limits of graft plasticity in terms of connectivity with the brain will help elucidate the efficiency with which forebrain organoids can integrate with different areas of the cortex.

Efferent projections from organoid grafts targeted many of the brain regions expected for the visual cortex[53] and observed for dissociated cell grafts inserted into the visual cortex, including the cortex, thalamus, and hippocampus.[27,37,38] Targets of the visual cortex that were not found included striatum and the midbrain, which is likely explained by the shorter time points examined in this study compared to other studies involving human neural grafts.[29] Off-target projections to areas such as the motor cortex and motor nuclei of the thalamus could be the result of neurons within the organoid grafts with non-occipital cortex identities. More investigation is needed to understand how graft efferents evolve over time, especially the process by which they are pruned. Similar to a prior study of embryonic rat cortical neuron transplantation,[27] organoid afferents primarily originated from cortex adjacent to the graft. Additional afferents were derived from the lateral geniculate nucleus of thalamus, the source of visual information to visual cortex, and bilateral hippocampi, which are known to project to the visual cortex.[54]

For both efferents and afferents, a framework for understanding the relative functional importance of the various connections between grafted neurons and the host brain does not currently exist. While some studies have touted the ability of transplanted neurons to form long-range connections with the brain,[5,21] local connections with adjacent cortex could in fact play a more relevant role in organoid graft integration, especially given their larger numbers. Establishing how different forms of graft-host connectivity contribute to the functional integration of the grafts will be important for developing strategies to augment and shape appropriate connectivity.

The spectrum of organoid integration with the host visual network

Our results demonstrate that it is possible for a human brain organoid to integrate functionally with the visual system of a host animal. A subset of organoid neurons exhibited feature selectivity, evidence of higher-order visual processing beyond simple evoked unit activity and LFPs. In the context of widespread disruption of cortical structure, this degree of integration has only been shown with rodent fetal cortical grafts,[8] which have restricted translational potential. Thus, our findings offer a path forward for using engineered neural tissues to rebuild visual cortex and restore function in conditions such as cortical blindness. Principles derived from this work likely will apply to repairing other regions of cortex as well.

It is important to keep in mind that our electrophysiological data present the spectrum of what is possible for organoid integration with the host brain rather than optimized integration. The percentage of organoid neurons that exhibited evidence of visual processing was lower than in the visual cortex, and the entire range of visual responses was not observed. As discussed above, improvements in generating cortical architecture *in vitro*, maintaining it after transplantation, and achieving more precise connectivity could produce a higher degree of and more consistent functional integration. Because vision contributes to the refinement and maturation of certain aspects of visual circuitry and neural function,[55,56] visual "rehabilitation" or neuromodulation of graft neurons could also improve their integration with the visual network. Lastly, consistent integration outcomes may require significant maturation of graft neurons. Even at 9 mpt, grafts of dissociated stem cell-derived human cortical neurons remain in a relatively immature state, likely reflecting human neoteny, and only 25% of examined neurons responded to light stimulation of the host animal.[28] Because of the extended timeline of human neurodevelopment, methods for accelerating graft maturation may be necessary to achieve the objective of neural tissue-based repair of cortical circuitry. Progress on these fronts will be necessary to achieve the ultimate objective of employing neural tissues as auxiliary cortical columns for rebuilding damaged cortical circuitry, which would have the added benefit of contributing to more sophisticated models of human brain development and diseases.[9,10,57,58]

Limitations of the study

Evaluation of histological and electrophysiological outcomes was limited to 3 months after organoid transplantation because of the limits of cyclosporine immunosuppression. Given the long periods of time needed for the maturation of human neurons,[28] it is likely that the graft neurons we evaluated were not completely mature. Longer time points after organoid transplantation would provide the opportunity to explore graft integration beyond the evoked responses we observed. This study utilized extracellular electrophysiology and chemogenetics to interrogate the functional integration of organoid grafts. While these approaches yielded robust data, additional insights into the functionality of organoid grafts could be gained from intracellular electrophysiology. Lastly, the aspiration cavity we created prior

to organoid insertion represents a significant brain injury but does not reflect the pathophysiology of disorders such as traumatic brain injury and stroke. Nonetheless, this approach provided proof of principle that organoid grafts could integrate with the injured adult mammalian brain.

STAR★METHODS

Detailed methods are provided in the online version of this paper and include the following:

- KEY RESOURCES TABLE
- RESOURCE AVAILABILITY
  - Lead contact
  - Materials availability
  - Data and code availability
- EXPERIMENTAL MODEL AND SUBJECT DETAILS
  - Human embryonic and induced pluripotent stem cells
  - Rat models and husbandry
  - Ethics statement
- METHOD DETAILS
  - Maintenance of stem cell lines
  - Generation of dorsal forebrain organoids
  - Organoid transplantation
  - Dissociation of brain organoids for transplantation
  - Transplantation of dissociated organoids
  - Modified rabies virus-based retrograde tracing
  - Herpes simplex virus-based anterograde tracing
  - Immunohistochemistry
  - Image analysis
  - Electrophysiology and visual stimulation
  - Neural signal analysis
- QUANTIFICATION AND STATISTICAL ANALYSIS

SUPPLEMENTAL INFORMATION

Supplemental information can be found online at https://doi.org/10.1016/j.stem.2023.01.004.

ACKNOWLEDGMENTS:

The authors thank Ashley Nemes, Nadir Bilici, and Madison O'Donnell for technical contributions and Magdalena Gotz for materials related to the modified rabies virus tracing system. This work was supported by the Department of Veterans Affairs, (IK2RX002013 to H.-C.I.C.), National Institutes of Health (R01NS119472 to H.-C.I.C., R35NS116843 to H.S., and R35NS097370 and RF1MH123979 to G.-l.M.), and the Dr. Miriam and Sheldon G. Adelson Medical Research Foundation (to G.-l.M.). Opinions, interpretations, and conclusions are those of the authors and are not necessarily endorsed by the Department of Veterans Affairs or the National Institutes of Health.

AUTHOR CONTRIBUTIONS

H.S., G.-l.M., and H.-C.I.C. conceived the study. J.L., Z.Z., P.H., F.J., and X.Q. generated the brain organoids and performed *in vitro* characterization experiments. D.J. performed animal surgeries and RABV injections. Z.Z. and D.J. performed HSV injections. Z.Z., P.H., S.S., J.B.G., R.B., and M.F. assisted with animal surgeries and performed related immunohistochemistry. J.G., K.M.-B., C.A., E.M., K.G., M.S., O.F., M.D., and I.R. performed *in vivo* electrophysiology experiments and related neural signal analysis. H.W. and F.X. constructed the HSV vector. D.J. and R.X. performed statistical analyses. J.A.W. and D.C. provided critical input for and oversight of the electrophysiology experiments. D.J. and H.-C.I.C. prepared the manuscript. D.C., J.A.W., H.S., and G.-l.M. provided critical feedback on the manuscript.

DECLARATION OF INTERESTS

G.-l.M. is on the editorial board of *Cell Stem* Cell.

Received: May 16, 2022
Revised: November 21, 2022
Accepted: January 11, 2023
Published: February 2, 2023

REFERENCES

1. Thurman, D.J., Alverson, C., Dunn, K.A., Guerrero, J., and Sniezek, J.E. (1999). Traumatic brain injury in the United States: A public health perspective. J. Head Trauma Rehabil. *14*, 602–615.
2. Hankey, G.J., Jamrozik, K., Broadhurst, R.J., Forbes, S., and Anderson, C.S. (2002). Long-term disability after first-ever stroke and related prognostic factors in the Perth Community Stroke Study, 1989-1990. Stroke *33*, 1034–1040.
3. Kempermann, G., Gage, F.H., Aigner, L., Song, H., Curtis, M.A., Thuret, S., Kuhn, H.G., Jessberger, S., Frankland, P.W., Cameron, H.A., et al. (2018). Human Adult Neurogenesis: Evidence and Remaining Questions. Cell Stem Cell *23*, 25–30. https://doi.org/10.1016/j.stem.2018.04.004.
4. Dancause, N., Barbay, S., Frost, S.B., Plautz, E.J., Chen, D., Zoubina, E.V., Stowe, A.M., and Nudo, R.J. (2005). Extensive cortical rewiring after brain injury. J. Neurosci. *25*, 10167–10179.
5. Gaillard, A., Prestoz, L., Dumartin, B., Cantereau, A., Morel, F., Roger, M., and Jaber, M. (2007). Reestablishment of damaged adult motor pathways by grafted embryonic cortical neurons. Nat. Neurosci. *10*, 1294–1299.
6. Santos-Torres, J., Heredia, M., Riolobos, A.S., Jimenez-Diaz, L., Gomez-Bautista, V., de la Fuente, A., Criado, J.M., Navarro-Lopez, J., and Yajeya, J. (2009). Electrophysiological and synaptic characterization of transplanted neurons in adult rat motor cortex. J. Neurotrauma *26*, 1593–1607.
7. Ballout, N., Frappe, I., Peron, S., Jaber, M., Zibara, K., and Gaillard, A. (2016). Development and Maturation of Embryonic Cortical Neurons Grafted into the Damaged Adult Motor Cortex. Front. Neural Circuits *10*, 55. https://doi.org/10.3389/fncir.2016.00055.
8. Girman, S.V., and Golovina, I.L. (1990). Electrophysiological properties of embryonic neocortex transplants replacing the primary visual cortex of adult rats. Brain Res. *523*, 78–86.
9. Chen, H.I., Song, H., and Ming, G.L. (2018). Applications of human brain organoids to clinical problems. Dev. Dyn. https://doi.org/10.1002/dvdy.24662.
10. Qian, X., Song, H., and Ming, G.L. (2019). Brain organoids: Advances, applications and challenges. Development *146*. https://doi.org/10.1242/dev.166074.
11. Kadoshima, T., Sakaguchi, H., Nakano, T., Soen, M., Ando, S., Eiraku, M., and Sasai, Y. (2013). Self-organization of axial polarity, inside-out layer pattern, and species-specific progenitor dynamics in human ES cell-derived neocortex. Proc. Natl. Acad. Sci. USA. *110*, 20284–20289. https://doi.org/10.1073/pnas.1315710110.
12. Pasca, A.M., Sloan, S.A., Clarke, L.E., Tian, Y., Makinson, C.D., Huber, N., Kim, C.H., Park, J.Y., O'Rourke, N.A., Nguyen, K.D., et al. (2015). Functional cortical neurons and astrocytes from human pluripotent stem cells in 3D culture. Nat. Methods *12*, 671–678. https://doi.org/10.1038/nmeth.3415.
13. Qian, X., Nguyen, H.N., Song, M.M., Hadiono, C., Ogden, S.C., Hammack, C., Yao, B., Hamersky, G.R., Jacob, F., Zhong, C., et al. (2016). Brain-Region-Specific Organoids Using Mini-bioreactors for Modeling ZIKV Exposure. Cell *165*, 1238–1254. https://doi.org/10.1016/j.cell.2016.04.032.
14. Qian, X., Su, Y., Adam, C.D., Deutschmann, A.U., Pather, S.R., Goldberg, E.M., Su, K., Li, S., Lu, L., Jacob, F., et al. (2020). Sliced Human Cortical

Organoids for Modeling Distinct Cortical Layer Formation. Cell Stem Cell *26*, 766–781.e9. https://doi.org/10.1016/j.stem.2020.02.002.

15. Lancaster, M.A., Corsini, N.S., Wolfinger, S., Gustafson, E.H., Phillips, A.W., Burkard, T.R., Otani, T., Livesey, F.J., and Knoblich, J.A. (2017). Guided self-organization and cortical plate formation in human brain organoids. Nat. Biotechnol. *35*, 659–666. https://doi.org/10.1038/nbt.3906.
16. Sloan, S.A., Darmanis, S., Huber, N., Khan, T.A., Birey, F., Caneda, C., Reimer, R., Quake, S.R., Barres, B.A., and Pasca, S.P. (2017). Human Astrocyte Maturation Captured in 3D Cerebral Cortical Spheroids Derived from Pluripotent Stem Cells. Neuron *95*, 779–790.e6. https://doi.org/10.1016/j.neuron.2017.07.035.
17. Marton, R.M., Miura, Y., Sloan, S.A., Li, Q., Revah, O., Levy, R.J., Huguenard, J.R., and Pasca, S.P. (2019). Differentiation and maturation of oligodendrocytes in human three-dimensional neural cultures. Nat. Neurosci. *22*, 484–491. https://doi.org/10.1038/s41593-018-0316-9.
18. Mansour, A.A., Goncalves, J.T., Bloyd, C.W., Li, H., Fernandes, S., Quang, D., Johnston, S., Parylak, S.L., Jin, X., and Gage, F.H. (2018). An in vivo model of functional and vascularized human brain organoids. Nat. Biotechnol. *36*, 432–441. https://doi.org/10.1038/nbt.4127.
19. Daviaud, N., Friedel, R.H., and Zou, H. (2018). Vascularization and Engraftment of Transplanted Human Cerebral Organoids in Mouse Cortex. eNeuro *5*, ENEURO.0219-18.2018. https://doi.org/10.1523/ENEURO.0219-18.2018.
20. Shi, Y., Sun, L., Wang, M., Liu, J., Zhong, S., Li, R., Li, P., Guo, L., Fang, A., Chen, R., et al. (2020). Vascularized human cortical organoids (vOrganoids) model cortical development in vivo. PLoS Biol. *18*, e3000705. https://doi.org/10.1371/journal.pbio.3000705.
21. Kitahara, T., Sakaguchi, H., Morizane, A., Kikuchi, T., Miyamoto, S., and Takahashi, J. (2020). Axonal Extensions along Corticospinal Tracts from Transplanted Human Cerebral Organoids. Stem Cell Rep. *15*, 467–481. https://doi.org/10.1016/j.stemcr.2020.06.016.
22. Wang, S.N., Wang, Z., Xu, T.Y., Cheng, M.H., Li, W.L., and Miao, C.Y. (2019). Cerebral Organoids Repair Ischemic Stroke Brain Injury. Transl. Stroke Res. *11*, 983–1000. https://doi.org/10.1007/s12975-019-00773-0.
23. Wang, Z., Wang, S.N., Xu, T.Y., Hong, C., Cheng, M.H., Zhu, P.X., Lin, J.S., Su, D.F., and Miao, C.Y. (2020). Cerebral organoids transplantation improves neurological motor function in rat brain injury. CNS Neurosci. Ther. *26*, 682–697. https://doi.org/10.1111/cns.13286.
24. Dong, X., Xu, S.B., Chen, X., Tao, M., Tang, X.Y., Fang, K.H., Xu, M., Pan, Y., Chen, Y., He, S., and Liu, Y. (2021). Human cerebral organoids establish subcortical projections in the mouse brain after transplantation. Mol. Psychiatry *26*, 2964–2976. https://doi.org/10.1038/s41380-020-00910-4.
25. Wilson, M.N., Thuneman, M., Liu, X., Lu, Y., Puppo, F., Adams, J.W., Kim, J., Pizzo, D.P., Djurovic, S., Andreassen, O.A., et al. (2022). Multimodal monitoring of human cortical organoids implanted in mice using transparent graphene microelectrodes reveal functional connection between organoid and mouse visual cortex. bioRxiv. https://doi.org/10.1101/2022.06.16.496469.
26. Revah, O., Gore, F., Kelley, K.W., Andersen, J., Sakai, N., Chen, X., Li, M.Y., Birey, F., Yang, X., Saw, N.L., et al. (2022). Maturation and circuit integration of transplanted human cortical organoids. Nature *610*, 319–326. https://doi.org/10.1038/s41586-022-05277-w.
27. Falkner, S., Grade, S., Dimou, L., Conzelmann, K.K., Bonhoeffer, T., Gotz, M., and Hubener, M. (2016). Transplanted embryonic neurons integrate into adult neocortical circuits. Nature *539*, 248–253. https://doi.org/10.1038/nature20113.
28. Linaro, D., Vermaercke, B., Iwata, R., Ramaswamy, A., Libe-Philippot, B., Boubakar, L., Davis, B.A., Wierda, K., Davie, K., Poovathingal, S., et al. (2019). Xenotransplanted Human Cortical Neurons Reveal Species-Specific Development and Functional Integration into Mouse Visual Circuits. Neuron *104*, 972–986.e976. https://doi.org/10.1016/j.neuron.2019.10.002.
29. Espuny-Camacho, I., Michelsen, K.A., Gall, D., Linaro, D., Hasche, A., Bonnefont, J., Bali, C., Orduz, D., Bilheu, A., Herpoel, A., et al. (2013). Pyramidal neurons derived from human pluripotent stem cells integrate efficiently into mouse brain circuits in vivo. Neuron *77*, 440–456. https://doi.org/10.1016/j.neuron.2012.12.011.
30. Martinez, L.M., Wang, Q., Reid, R.C., Pillai, C., Alonso, J.M., Sommer, F.T., and Hirsch, J.A. (2005). Receptive field structure varies with layer in the primary visual cortex. Nat. Neurosci. *8*, 372–379. https://doi.org/10.1038/nn1404.
31. Self, M.W., van Kerkoerle, T., Goebel, R., and Roelfsema, P.R. (2019). Benchmarking laminar fMRI: Neuronal spiking and synaptic activity during top-down and bottom-up processing in the different layers of cortex. Neuroimage *197*, 806–817. https://doi.org/10.1016/j.neuroimage.2017.06.045.
32. Raizada, R.D., and Grossberg, S. (2003). Towards a theory of the laminar architecture of cerebral cortex: computational clues from the visual system. Cereb. Cortex *13*, 100–113.
33. Mo, Z., and Zecevic, N. (2008). Is Pax6 critical for neurogenesis in the human fetal brain? Cereb. Cortex *18*, 1455–1465. https://doi.org/10.1093/cercor/bhm181.
34. Su, Y., Zhou, Y., Bennett, M.L., Li, S., Carceles-Cordon, M., Lu, L., Huh, S., Jimenez-Cyrus, D., Kennedy, B.C., Kessler, S.K., et al. (2022). A single-cell transcriptome atlas of glial diversity in the human hippocampus across the postnatal lifespan. Cell Stem Cell *29*, 1594–1610.e8. https://doi.org/10.1016/j.stem.2022.09.010.
35. von Bartheld, C.S., Bahney, J., and Herculano-Houzel, S. (2016). The search for true numbers of neurons and glial cells in the human brain: A review of 150 years of cell counting. J. Comp. Neurol. *524*, 3865–3895. https://doi.org/10.1002/cne.24040.
36. Gaillard, A., Nasarre, C., and Roger, M. (2003). Early (E12) cortical progenitors can change their fate upon heterotopic transplantation. Eur. J. Neurosci. *17*, 1375–1383.
37. Espuny-Camacho, I., Michelsen, K.A., Linaro, D., Bilheu, A., Acosta-Verdugo, S., Herpoel, A., Giugliano, M., Gaillard, A., and Vanderhaeghen, P. (2018). Human Pluripotent Stem-Cell-Derived Cortical Neurons Integrate Functionally into the Lesioned Adult Murine Visual Cortex in an Area-Specific Way. Cell Rep. *23*, 2732–2743. https://doi.org/10.1016/j.celrep.2018.04.094.
38. Michelsen, K.A., Acosta-Verdugo, S., Benoit-Marand, M., Espuny-Camacho, I., Gaspard, N., Saha, B., Gaillard, A., and Vanderhaeghen, P. (2015). Area-specific reestablishment of damaged circuits in the adult cerebral cortex by cortical neurons derived from mouse embryonic stem cells. Neuron *85*, 982–997. https://doi.org/10.1016/j.neuron.2015.02.001.
39. Wickersham, I.R., Lyon, D.C., Barnard, R.J., Mori, T., Finke, S., Conzelmann, K.K., Young, J.A., and Callaway, E.M. (2007). Monosynaptic restriction of transsynaptic tracing from single, genetically targeted neurons. Neuron *53*, 639–647. https://doi.org/10.1016/j.neuron.2007.01.033.
40. Sun, N., Cassell, M.D., and Perlman, S. (1996). Anterograde, transneuronal transport of herpes simplex virus type 1 strain H129 in the murine visual system. J. Virol. *70*, 5405–5413. https://doi.org/10.1128/JVI.70.8.5405-5413.1996.
41. Tornero, D., Tsupykov, O., Granmo, M., Rodriguez, C., Gronning-Hansen, M., Thelin, J., Smozhanik, E., Laterza, C., Wattananit, S., Ge, R., et al. (2017). Synaptic inputs from stroke-injured brain to grafted human stem cell-derived neurons activated by sensory stimuli. Brain *140*, 692–706. https://doi.org/10.1093/brain/aww347.
42. Palma-Tortosa, S., Tornero, D., Gronning Hansen, M., Monni, E., Hajy, M., Kartsivadze, S., Aktay, S., Tsupykov, O., Parmar, M., Deisseroth, K., et al. (2020). Activity in grafted human iPS cell-derived cortical neurons integrated in stroke-injured rat brain regulates motor behavior. Proc. Natl. Acad. Sci. USA. *117*, 9094–9100. https://doi.org/10.1073/pnas.2000690117.
43. Trujillo, C.A., Gao, R., Negraes, P.D., Gu, J., Buchanan, J., Preissl, S., Wang, A., Wu, W., Haddad, G.G., Chaim, I.A., et al. (2019). Complex Oscillatory Waves Emerging from Cortical Organoids Model Early Human Brain Network Development. Cell Stem Cell. https://doi.org/10.1016/j.stem.2019.08.002.

44. Birey, F., Andersen, J., Makinson, C.D., Islam, S., Wei, W., Huber, N., Fan, H.C., Metzler, K.R.C., Panagiotakos, G., Thom, N., et al. (2017). Assembly of functionally integrated human forebrain spheroids. Nature *545*, 54–59. https://doi.org/10.1038/nature22330.

45. Xiang, Y., Tanaka, Y., Patterson, B., Kang, Y.J., Govindaiah, G., Roselaar, N., Cakir, B., Kim, K.Y., Lombroso, A.P., Hwang, S.M., et al. (2017). Fusion of Regionally Specified hPSC-Derived Organoids Models Human Brain Development and Interneuron Migration. Cell Stem Cell *21*, 383–398.e7. https://doi.org/10.1016/j.stem.2017.07.007.

46. Samarasinghe, R.A., Miranda, O.A., Buth, J.E., Mitchell, S., Ferando, I., Watanabe, M., Allison, T.F., Kurdian, A., Fotion, N.N., Gandal, M.J., et al. (2021). Identification of neural oscillations and epileptiform changes in human brain organoids. Nat. Neurosci. *24*, 1488–1500. https://doi.org/10.1038/s41593-021-00906-5.

47. Basuodan, R., Basu, A.P., and Clowry, G.J. (2018). Human neural stem cells dispersed in artificial ECM form cerebral organoids when grafted in vivo. J. Anat. *233*, 155–166. https://doi.org/10.1111/joa.12827.

48. Carlson, A.L., Bennett, N.K., Francis, N.L., Halikere, A., Clarke, S., Moore, J.C., Hart, R.P., Paradiso, K., Wernig, M., Kohn, J., et al. (2016). Generation and transplantation of reprogrammed human neurons in the brain using 3D microtopographic scaffolds. Nat. Commun. *7*, 10862. https://doi.org/10.1038/ncomms10862.

49. Francis, N.L., Zhao, N., Calvelli, H.R., Saini, A., Gifford, J.J., Wagner, G.C., Cohen, R.I., Pang, Z.P., and Moghe, P.V. (2019). Peptide-Based Scaffolds for the Culture and Transplantation of Human Dopaminergic Neurons. Tissue Eng. Part A *26*, 193–205. https://doi.org/10.1089/ten.TEA.2019.0094.

50. Gaspard, N., Bouschet, T., Hourez, R., Dimidschstein, J., Naeije, G., van den Ameele, J., Espuny-Camacho, I., Herpoel, A., Passante, L., Schiffmann, S.N., et al. (2008). An intrinsic mechanism of corticogenesis from embryonic stem cells. Nature *455*, 351–357. https://doi.org/10.1038/nature07287.

51. Gaillard, A., and Roger, M. (2000). Early commitment of embryonic neocortical cells to develop area-specific thalamic connections. Cereb. Cortex *10*, 443–453.

52. Barbe, M.F., and Levitt, P. (1995). Age-dependent specification of the corticocortical connections of cerebral grafts. J. Neurosci. *15*, 1819–1834.

53. Oh, S.W., Harris, J.A., Ng, L., Winslow, B., Cain, N., Mihalas, S., Wang, Q., Lau, C., Kuan, L., Henry, A.M., et al. (2014). A mesoscale connectome of the mouse brain. Nature *508*, 207–214. https://doi.org/10.1038/nature13186.

54. Cenquizca, L.A., and Swanson, L.W. (2007). Spatial organization of direct hippocampal field CA1 axonal projections to the rest of the cerebral cortex. Brain Res. Rev. *56*, 1–26. https://doi.org/10.1016/j.brainresrev.2007.05.002.

55. White, L.E., Coppola, D.M., and Fitzpatrick, D. (2001). The contribution of sensory experience to the maturation of orientation selectivity in ferret visual cortex. Nature *411*, 1049–1052. https://doi.org/10.1038/35082568.

56. Hooks, B.M., and Chen, C. (2006). Distinct roles for spontaneous and visual activity in remodeling of the retinogeniculate synapse. Neuron *52*, 281–291. https://doi.org/10.1016/j.neuron.2006.07.007.

57. Kelava, I., and Lancaster, M.A. (2016). Dishing out mini-brains: Current progress and future prospects in brain organoid research. Dev. Biol. *420*, 199–209. https://doi.org/10.1016/j.ydbio.2016.06.037.

58. Di Lullo, E., and Kriegstein, A.R. (2017). The use of brain organoids to investigate neural development and disease. Nat. Rev. Neurosci. *18*, 573–584. https://doi.org/10.1038/nrn.2017.107.

59. Su, P., Ying, M., Han, Z., Xia, J., Jin, S., Li, Y., Wang, H., and Xu, F. (2020). High-brightness anterograde transneuronal HSV1 H129 tracer modified using a Trojan horse-like strategy. Mol. Brain *13*, 5. https://doi.org/10.1186/s13041-020-0544-2.

60. Wen, Z., Nguyen, H.N., Guo, Z., Lalli, M.A., Wang, X., Su, Y., Kim, N.S., Yoon, K.J., Shin, J., Zhang, C., et al. (2014). Synaptic dysregulation in a human iPS cell model of mental disorders. Nature *515*, 414–418. https://doi.org/10.1038/nature13716.

61. Chiang, C.H., Su, Y., Wen, Z., Yoritomo, N., Ross, C.A., Margolis, R.L., Song, H., and Ming, G.L. (2011). Integration-free induced pluripotent stem cells derived from schizophrenia patients with a DISC1 mutation. Mol. Psychiatry *16*, 358–360. https://doi.org/10.1038/mp.2011.13.

62. Paluru, P., Hudock, K.M., Cheng, X., Mills, J.A., Ying, L., Galvao, A.M., Lu, L., Tiyaboonchai, A., Sim, X., Sullivan, S.K., et al. (2014). The negative impact of Wnt signaling on megakaryocyte and primitive erythroid progenitors derived from human embryonic stem cells. Stem Cell Res. *12*, 441–451. https://doi.org/10.1016/j.scr.2013.12.003.

63. Chen, Y., Xiong, M., Dong, Y., Haberman, A., Cao, J., Liu, H., Zhou, W., and Zhang, S.C. (2016). Chemical Control of Grafted Human PSC-Derived Neurons in a Mouse Model of Parkinson's Disease. Cell Stem Cell *18*, 817–826. https://doi.org/10.1016/j.stem.2016.03.014.

64. McQuin, C., Goodman, A., Chernyshev, V., Kamentsky, L., Cimini, B.A., Karhohs, K.W., Doan, M., Ding, L., Rafelski, S.M., Thirstrup, D., et al. (2018). CellProfiler 3.0: Next-generation image processing for biology. PLoS Biol. *16*, e2005970. https://doi.org/10.1371/journal.pbio.2005970.

65. Tang, J., Ardila Jimenez, S.C., Chakraborty, S., and Schultz, S.R. (2016). Visual Receptive Field Properties of Neurons in the Mouse Lateral Geniculate Nucleus. PLoS One *11*, e0146017. https://doi.org/10.1371/journal.pone.0146017.

STAR★METHODS

KEY RESOURCES TABLE

REAGENT or RESOURCE	SOURCE	IDENTIFIER
Antibodies		
Caspase 3	Abcam	Cat# ab2302; RRID: AB_302962
CD3	Abcam	Cat# ab237721
CD31	Abcam	Cat# ab28364; RRID: AB_726362
CD68	Abcam	Cat# ab125212; RRID: AB_10975465
Coup-TF1	R&D Systems	Cat# PP-H8132-00; RRID: AB_2155494
CTIP2	Abcam	Cat# ab28448; RRID: AB_1140055
Cux1	Santa Cruz	Cat# sc-13024; RRID: AB_2261231
FoxG1	Abcam	Cat# ab18259; RRID: AB_732415
GFAP	Chemicon	Cat# 04-1031; RRID: AB_11214219
Iba1	Fujifilm Wako	Cat# 019-19741; RRID: AB_839504
Ki67	Abcam	Cat# ab15580; RRID: AB_443209
Map2	Abcam	Cat# ab11267; RRID: AB_297885
MBP	Invitrogen	Cat# MA1-10837; RRID: AB_1077025
Necab1	Novus Biologicals	Cat# NBP1-84004; RRID: AB_11025438
NeuN	Abcam	Cat# ab177487; RRID: AB_2532109
Olig2	Chemicon	Cat# ab9610
Pax6	Biolegend	Cat# 901301; RRID: AB_2565003
Satb2	Abcam	Cat# ab51502; RRID: AB_882455
STEM121	Takara Bio	Cat# Y40410; RRID: AB_2801314
Sox2	Abcam	Cat# ab97959; RRID: AB_2341193
Sp8	Santa Cruz	Cat# sc-104661
Synapsin	Synaptic Systems	Cat# 106-001; RRID: AB_887805
Tau	Abcam	Cat# ab92676; RRID: AB_10561457
Tbr1	Abcam	Cat# ab31940; RRID: AB_2200219
IgG (H+L) Cross-Adsorbed Goat anti-Mouse, Alexa Fluor 488	Invitrogen	Cat# A32723; RRID: AB_2633275
Goat anti-Rabbit IgG (H+L) Cross-Adsorbed Secondary Antibody, Alexa Fluor 647	Invitrogen	Cat# A21244; RRID: AB_2535812
Goat Anti-Mouse IgG H&L (Alexa Fluor 647)	Abcam	Cat# ab150115; RRID: AB_2687948
IgG (H+L) Cross-Adsorbed Goat anti-Rabbit, Alexa Fluor 555	Invitrogen	Cat# A21428; RRID: AB_141784
IgG (H+L) Highly Cross-Adsorbed Donkey anti-Rabbit, Alexa Fluor 594	Invitrogen	Cat# A21207; RRID: AB_141637
Bacterial and virus strains		
RVdG-EGFP	BrainVTA	Cat#R01001
HSV-GFP	Su et al.[59]	N/A
Biological samples		
Human WT iPSC line "C1–2" derived from healthy fibroblasts (male)	ATCC fibroblasts (CRL-2097); Wen et al.[60]	C1–2
H9-GFP (female)	WiCell Research Institute	LT2e-H9CAGGFP
AICS iPSC line (male)	Allen Cell Collection at Coriell	GM25256
Isogenic human iPSC line derived from "C1-2", modified by lentiviral transduction to express the RABV tracing mechanism (DsRed-G-TVA800)	ATCC fibroblasts (CRL-2097); Wen et al.[60]	C1.2-DsRedExp2-G-TVA

(*Continued on next page*)

Continued		
REAGENT or RESOURCE	SOURCE	IDENTIFIER
H9CAGhM4Di (female)	WiCell Research Institute	H9-hM4Di
RVdG-EGFP	BrainVTA	Cat#R01001
HSV-GFP	Su et al.[59]	N/A
Chemicals, peptides, and recombinant proteins		
DMEM:F12	Invitrogen	cat. # 11330032
Neurobasal medium	GIBCO	cat. # 21103049
PBS	GIBCO	cat. # 10010023
KnockOut Serum Replacement	GIBCO	cat. # 10828028
Non-essential Amino Acids	GIBCO	cat. # 11140050
Penicillin/Streptomycin	GIBCO	cat. # 15140122
2-Mercaptoenthanol	GIBCO	cat. # 21985023
GlutaMAX	GIBCO	cat. # 35050061
Collagenase Type IV	Invitrogen	cat. # 17104019
FGF-2	Peprotech	cat. # 100–18B
Dorsomorphine	StemCell Technologies	cat. # 72102
A83–01	StemCell Technologies	cat. # 72022
N2 Supplement	GIBCO	cat. # 17502048
B27 Supplements	GIBCO	cat. # 17504044
CHIR99021	StemCell Technologies	cat. # 72052
SB-431542	StemCell Technologies	cat. # 72232
BDNF	Peprotech	cat. # 450–02
GDNF	Peprotech	cat. # 450–10
Paraformaldehyde	Polysciences	cat. # 18814–10
Aqua-PolyMount	Polysciences	cat. # 18606-100
Clozapine-N-oxide	Enzo Life Sciences	cat. # 50-103-1781
Experimental models: Cell lines		
Human WT iPSC line "C1–2" derived from healthy fibroblasts (male)	ATCC fibroblasts (CRL-2097); Wen et al.[60]	C1–2
H9-GFP (female)	WiCell Research Institute	LT2e-H9CAGGFP
AICS iPSC line (male)	Allen Cell Collection at Coriell	GM25256
Isogenic human iPSC line derived from "C1-2", modified by lentiviral transduction to express the RABV tracing mechanism (DsRed-G-TVA800)	ATCC fibroblasts (CRL-2097); Wen et al.[60]	C1.2-DsRedExp2-G-TVA
H9CAGhM4Di (female)	WiCell Research Institute	H9-hM4Di
Experimental models: Organisms/strains		
Rat (Long Evans)	Charles River	006
Recombinant DNA		
EnvA-pseudotyped RVdG-eGFP	The Vector Core at the Salk Institute	N/A
Software and algorithms		
ImageJ (Fiji)	NIH	https://imagej.nih.gov/ij/docs/guide/146–2.html
GraphPad Prism (8.0)	GraphPad	https://www.graphpad.com/scientific-software/prism/
Microsoft Excel	Microsoft	https://www.microsoft.com/en-us/p/excel/cfq7ttc0k7dx?activetab=pivot%3aoverviewtab

RESOURCE AVAILABILITY

Lead contact

Further information and requests for resources and reagents should be directed to and will be fulfilled by the lead contact, Han-Chiao Isaac Chen (Isaac.Chen@pennmedicine.upenn.edu).

Materials availability

All biological materials used in this study are available from the lead contact upon request or from commercial sources.

Data and code availability

- All data reported in this paper will be shared by the lead contact upon request.
- This paper does not report original code.
- Any additional information required to reanalyze the data reported in this paper is available from the lead contact upon request.

EXPERIMENTAL MODEL AND SUBJECT DETAILS

Human embryonic and induced pluripotent stem cells

Three pluripotent stem cell lines were used in this study, including two iPS cell lines (C1.2[61] and AICS-GFP-0036 [Coriell Institute for Medical Research]) and one ES cell line (H9 [WiCell]). Variations of these lines are described below. The H9 line expressing enhanced green fluorescent protein driven by the chicken beta-actin promoter (H9-GFP) was generated using zinc finger nucleases to target the expression construct to the AAVS1 locus (Children's Hospital of Philadelphia Stem Cell Core).[62] The H9 line expressing hM4Di, an inhibitory designer receptor exclusively activated by designer drugs (DREADD), fused to mCherry and driven the CAG promoter (H9-hM4Di) was generated by targeting the AAVS1 locus using CRISPR techniques.[63] The C1.2-GFP and C1.2-DsRedExp2-G-TVA lines were created via lentiviral transduction of the C1.2 line with constructs driven by the cytomegalovirus and chicken beta-actin promoters, respectively.

Rat models and husbandry

Young adult Long Evans rats (male, 250-300 g, 8-12 weeks) were immunosuppressed with cyclosporine A (intraperitoneal [IP], 10 mg/kg; Novartis) for 2 days prior to organoid transplantation. All animal experiments described in this study were approved by the Institutional Animal Care and Use Committee (IACUC) at the University of Pennsylvania and were conducted in accordance with the National Institutes of Health's Guide for the Care and Use of Laboratory Animals. Animals were housed in pairs under standard conditions and kept on a 12-h light/dark cycle (lights on at 6:00 a.m.) with *ad libitum* access to food and water.

Ethics statement

The use of previously generated human pluripotent stem cell lines and the xenotransplantation of human brain organoids in this study was reviewed and approved by the Stem Cell Research Oversight Committee at the University of Pennsylvania.

METHOD DETAILS

Maintenance of stem cell lines

Cells were grown as colonies on a feeder layer of irradiated mouse embryonic fibroblasts (MEFs; Gibco). Daily media changes were performed with hES cell media, which consisted of Dulbecco's modified Eagle's medium (DMEM)/F12 (Gibco) supplemented with 20% knockout serum replacement (KOSR, Gibco), 100 U/mL penicillin and 100 mg/mL streptomycin (Gibco), 2mM GlutaMAX (Gibco), 0.1 mM non-essential amino acids (NEAA; Gibco), 100 mM β-mercaptoethanol (Gibco), and 6 ng/mL basic fibroblast growth factor (bFGF, R&D Systems). Stem cell cultures were maintained in 6-well tissue culture plates and passaged at a ratio of 1:10 every 4–6 days using 300 U/ml collagenase type IV (Gibco). Stem cell lines were maintained below passage number 50 and confirmed to be negative for mycoplasma using a universal mycoplasma detection kit (ATCC) on a monthly basis.

Generation of dorsal forebrain organoids

Forebrain organoids were generated using a modified version of our previously published protocol[13] In brief, embryoid bodies (EBs) were created by detaching stem cell colonies using 300 U/mL collagenase type IV. From day 0–4, detached colonies were cultured in ultra low-attachment 6-well plates (Corning Costar) in DMEM/F12 media, 20% Knockout Serum Replacement (KSR), 2 mM GlutaMAX, 0.1 mM NEAA, 94.6 μM β-mercaptoethanol, 200 nM LDN193189 (Tocris), and 10 μM SB431542 (Tocris). On days 5 and 6, the media was half-changed to induction media (IM) consisting of DMEM/D12 with 1X N2 supplement (Gibco), 0.1 mM non-essential amino acids, 2 mM GlutaMAX, 1 μM CHIR 99021 (Tocris), 1 μM SB431542 (Tocris), and 100 U/mL penicillin and 100 ng/mL streptomycin. On day 7, EBs were embedded in a 1:1 Matrigel (Corning) to IM mixture. This mixture was maintained on ice, and EBs were dispersed throughout it by gentle pipetting. The Matrigel and embedded EBS were then spread on an ultra-low attachment 6-well plate and allowed to gel at 37°C for 30 min. The embedded EBs were then cultured in stationary conditions

in IM media from day 7-14. On day 14, the embedded EBs were gently broken out of the Matrigel hydrogel with a 5-mL serological pipette and transferred to an orbital shaker (100-120 rpm). From day 14–71, the organoids were cultured in differentiation media consisting of 50% DMEM/F12 and 50% Neurobasal medium (Gibco) with 1X N2 supplement, 1X B27 supplement (Gibco), 2 mM GlutaMAX, 2.8 ng/mL human insulin (Sigma), 0.1 mM NEAA, 100 μM β-mercaptoethanol, and 100 U/mL penicillin and 100 ng/mL streptomycin. Media changes were performed every 2 days. Thereafter, the organoids were maintained in maturation media consisting of Neurobasal with 1X B27 supplement, 2 mM GlutaMax, 0.2 mM ascorbic acid, 20 ng/mL brain-derived neurotrophic factor (PeproTech), 20 ng/mL glial cell line-dervied neurotrophic factor (PeproTech), and 50 U/mL penicillin and 50 ng/mL streptomycin. Media changes were performed every 2 days.

Only organoids that passed strict quality control were selected for subsequent transplantation. Metrics that were assessed including the clearing of embryoid body borders before Matrigel embedding suggestive of the formation of radially organized neuroepithelium and the development of defined buds in Matrigel without cyst formation or evidence of premature differentiation.

Organoid transplantation

All animal experiments described in this study were approved by the IACUC at the University of Pennsylvania (protocol number 805600) and were conducted in accordance with the National Institutes of Health's Guide for the Care and Use of Laboratory Animals. Animals were housed in pairs under standard conditions and kept on a 12-h light/dark cycle (lights on at 6:00 a.m.) with *ad libitum* access to food and water.

Young adult Long Evans rats (male, 250-300 g, 8-12 weeks) were immunosuppressed with cyclosporine A (intraperitoneal [IP], 10 mg/kg; Novartis) for 2 days prior to organoid transplantation. On the day of transplantation, general anesthesia was induced with isoflurane, and the animals were mounted on a stereotaxic frame. Pre-operative medications given included dexamethasone (IP, 1 mg/kg; Mylan) to decrease cerebral edema and bupivacaine (SC, 2 mg/kg; APP Pharmaceuticals) for local anesthesia at the site of surgery. Isoflorane was maintained at 2–2.5%, and body temperature was supported using a water circulation-based heating bad (Gaymar). The depth of anesthesia was assessed by monitoring animal respirations as well as toe pinch responses every 10 min during the surgery. A 5- mm circular craniotomy centered at AP: 5 mm posterior to bregma and ML: 2.5 mm was performed manually with a hand-held drill. A durotomy was performed, and a cortical cavity was created in the center of the craniotomy using vacuum aspiration (diameter to fit the organoid being transplanted, depth of 2 mm). Meticulous hemostasis was achieved, after which a day 80-88 organoid was transferred into the cortical cavity. Organoid grafts were incubated with 20 μg/mL necrostatin-1 (Enzo Life Sciences) for 24 h prior to transplantation. A custom polydimethylsiloxane (PDMS; Dow Silicones Corporation) cranioplasty cap was placed in the craniotomy defect and sealed in place with polymethylmethacrylate (PMMA; Densply). The skin was then closed with suture. Post-operatively, animals were given daily SC injections of meloxicam (1 mg/kg; Norbrook) over 2 days for systemic pain control. Daily IP injections of cyclosporine A were performed until sacrifice to maintain immunosuppression. Animals were survived for 1, 2, or 3 months after transplantation for histological and electrophysiological studies and 2 months for virus-based tracing studies.

Dissociation of brain organoids for transplantation

After incubation with 20 μg/mL necrostatin-1 for 24 h, C1.2-GPF organoids at dd80 were dissociated into a single cell suspension as follows. Individual organoids were washed incubated with Accutase (Gibco) in a conical tube at 37°C for 20 min. A 1 mL pipette tip was then used to mechanically dissociate the organoids. The cell suspension was then centrifuged at 300 g for 5 min, resuspended in 2mL of DNase I solution (1 mg/mL, STEMCELL), and incubated at 37°C for 5 min. Quenching of DNAse I activity was performed by the addition of 8 mL of maturation media. The cell suspension was again centrifuged at 300 g for 5 min and resuspended in media for cell culture or 10 μL of normal saline solution per organoid for transplantation.

Transplantation of dissociated organoids

The transplantation methodology for dissociated organoids was largely the same as what is described in the organoid transplantation section above, with the following differences. The injury cavity was kept constant at 2 mm in diameter and 2 mm in depth. After hemostasis had been achieved, the high-density cell suspension (cells from 1 organoid in 10 μL) was deposited into the cortical cavity over 1 min using a pipette. The cells were allowed to settle within the cortical cavity for 15-20 min before closing the craniotomy defect as described above.

Modified rabies virus-based retrograde tracing

Animals transplanted with organoids expressing the modified RABV retrograde tracing mechanism (C1.2-DsRedExp2-G-TVA line) were anesthetized with isoflurane 7-10 days prior to the designated timepoint and mounted on a stereotaxic frame. The prior skin incision was opened, and the PDMS/PMMA cranioplasty was removed. The fluorescent organoid graft was visualized using ultraviolet (UV) light. A 32G Hamilton syringe connected to a micro-injection pump (WPI) then was used to inject a modified RABV expressing GFP in place of the RABV glycoprotein (1.08×10^8 transforming units/mL, Salk Institute) into the organoid graft. Three injections (200 mL of virus per injection site) were performed at a rate of 20 nL/min with injection sites 500 μm apart in a triangular shape. A new PDMS/PMMA cranioplasty was fashioned, and the skin was closed with suture. The animals were sacrificed at the designated time point by transcardial perfusion.

Herpes simplex virus-based anterograde tracing

Animals transplanted with non-fluorescent C1.2 organoids were anesthetized 7-10 days prior to the designated time point and mounted on a stereotaxic frame. Subsequently, a pulled glass pipette attached to a Nanoject III pump (Drummond) was used to perform an intravitreal injection of HSV expressing GFP ($5.9x10^9$ plaque-forming units/mL, 1.5 μL) into the host animal's eye that was contralateral to the organoid graft. Details of the construction of the HSV-GFP vector have been published previously.[59] The animals were sacrificed at the designated time point by transcardial perfusion.

Immunohistochemistry

At the designated timepoints, animals were euthanized with a lethal dose of Euthasol (>150 mg/kg IP; Virbac). The animals were then perfused transcardially with 0.9% NaCl solution supplemented with heparin (1 United States Pharmacopeia [USP] unit/mL; Sagent) followed by 10% formalin. Extracted brains and *in vitro* brain organoids were post-fixed with 10% formalin for 24 h at 4°C and then immersed in 30% sucrose for 72 h at 4°C for cryoprotection. The brains and organoids were then flash-frozen in isopentane at −40°C, and 25-μm coronal sections were collected using a cryostat. Tissue sections were stored at −20°C until use.

Prior to immunostaining, tissue sections were dried at room temperature for 10 min, rehydrated with tris-buffered saline with 0.1% Tween 20 (TBST) for 1 h, and then washed 3 times with TBST (10 min per wash). Blocking and permeabilization were performed with TBST with 5% normal goat serum (NGS; Vector Labs) and 0.3% Triton X-100 (Sigma) for 1 h at room temperature. Primary antibodies diluted in 5% NGS/TBST were applied to tissue sections overnight at 4°C. The following day, three rinses with TBST (10 min each) were performed, after which the tissue sections were incubated with the appropriate Alexa Fluor secondary antibody (Thermo Fisher Scientific) diluted in 5% NGS/TBST for 2 h at room temperature. The samples were then rinsed another three times before coverslips were mounted with Aqua-PolyMount (Polysciences, Inc.).

Image analysis

Imaging was performed using a Nikon A1plus confocal system and NIS-Elements AR software (Nikon). The NIS-Elements AR software was utilized to automatically stitch together individual images with a 25% overlap of the field of view. Analysis was performed using the Fiji package of ImageJ software (U.S. National Institutes of Health).

For quantification of organoid survival rates, the presence of any fluorescent signal associated with the organoid graft, irrespective of size, was considered to be evidence of organoid survival.

For quantification of organoid graft volumes, the GFP^+ area of every fourth section was measured. Images were acquired using a 4x objective, and the GFP^+ area was selected using the thresholding feature in Fiji. Thresholding was adjusted to visualize only the GFP signal, and the same settings were applied to all images. The GFP + area of unimaged sections was estimated using the assumption that area scaled in a linear fashion between two measured sections. Each area (measured and estimated) was multiplied by the thickness of the sections (i.e., 25 μm), and these volumes were summated to determine the volume of an organoid graft.

For quantification of immunostaining markers within organoid grafts, images of the entire organoid were acquired in every 10^{th} section of the organoid using a 20X objective. Every 10^{th} section was chosen for analysis to accommodate the large number of antibody combinations included in this study. Between 12-18 sections (median of 15 sections) were used for histological analyses of the organoid grafts. Multiple images of the organoid were stitched together by overlapping 10% of the acquired images. The area of the entire organoid was then analyzed. For quantification of the host brain adjacent to the graft, every 10th section of the organoid was imaged as above after which a 200 μm band of host tissue was demarcated based on a manually defined host-graft border and cropped for further analysis. The area of this entire band of host brain was then analyzed. Counting was performed using the cell counting software Cell Profiler for Cells.[64]

Quantification of organoid graft projections and RABV/HSV tracing was performed in every 10^{th} section of the brain. Sections were stained with a GFP antibody to amplify the GFP signal. The Paxinos and Watson atlas (sixth edition) was used to determine the location of different brain regions in 4x images of sections by overlaying the atlas images over the acquired images. Brain regions containing GFP^+ processes or cells were identified, and regions of interest were established for each brain region to be quantified. The GFP^+ area was calculated as the GFP^+ area divided by the total area of the ROI. GFP^+ cells were quantified by manually counting the number of GFP^+ cells in the entirety of each brain region.

For electrode track identification, manual evaluation of every section was performed to find the location of all electrode tracks. This process was aided by the logs of electrode track locations and depths that were made during electrophysiological recordings. Examples of electrode tracks are presented in Figures S7A-D. Data from electrodes that were located 100 μm or closer to the graft-host brain interface were excluded from analyses to minimize the risk of contamination from normal brain activity.

Electrophysiology and visual stimulation

Neural recordings were obtained in anesthetized animals transplanted with GFP + organoids. General anesthesia was induced using isoflurane, and animals were mounted on a stereotaxic frame. The prior incision was opened, and the PDMS/PMMA cranioplasty was removed. The presence of a surviving organoid graft was confirmed using UV light. Reference and ground screws (McMaster-Carr) were inserted into the skull overlying the cerebellum, and a multichannel silicon probe (32 channels, H6B; Cambridge Neurotechnologies) was inserted into the host cortex at least 1 mm away from the edge of the graft. The dose of isoflurane was gradually decreased

until a plane of anesthesia was achieved that supported a desynchronized brain state. A second silicon probe was then inserted into the organoid using UV light to differentiate the graft from the host brain. Recordings acquired at 32 kHz were amplified with a headstage (HS-32; Neuralynx). If no unit activity was identified, the probe was advanced deeper into the organoid along the same track or placed in a different position to create a new track. If spontaneous activity was observed on the organoid probe, activity was recorded for a baseline period of at least 5 min. Next, a 24″ LED monitor with 1920x1080 resolution and a 144 Hz refresh rate (ASUS) was positioned 30 cm from the host animal's eye contralateral to the side of the organoid graft (60 degrees off midline, 15° above the horizon). Whole-screen flashing light stimulation was presented (0.5 Hz, 50 ms pulse width), and evoked activity was recorded from both the organoid and brain probes for 5 min. After completion of the flashing light paradigm, full-screen drifting gratings were displayed using the same monitor. Eight orientations of drifting gratings (0°, 45°, 90°, 135°, 180°, 225°, 270°, 315°) with a spatial frequency of 0.08 cycles per degree and a speed of 2 cycles per s were generated using the MATLAB Psychophysics Toolbox and displayed for 15 s followed by a gray screen for 5 s. The 8 orientations were randomly permuted to generate a single trial block. Three to ten blocks were presented at each recording site. A mean of 3.4 electrode tracks were performed in each organoid (range 2-5), and recordings were obtained from a mean of 1.62 sites per track (range 1-3).

For chemogenetic studies, organoids derived from the H9-HM4Di line were transplanted into cortical aspiration cavities as described above. Recordings of spontaneous activity and activity evoked by light stimulation were performed at baseline before CNO administration. Subsequently, intraperitoneal CNO (3 mg/kg, Enzo Life Sciences) was given, and spontaneous activity was again recorded up to 2 h after CNO administration.

Neural signal analysis

Neural recordings were processed offline. If multiple recordings were performed at a single depth (e.g., baseline and visual stimulation), recordings were merged prior to spike sorting. For sorting of single units, the recorded spike waveforms were imported into SpikeSort 3D (version 2.5.4; Neuralynx). Unit activity was first identified through Klustakwik automatic cluster detection along a five-dimensional feature vector including two peak and three valley features. Automatically generated clusters were merged, split, or discarded as appropriate. The resultant clusters then were optimized via manual thresholding. Isolated signals were confirmed as single units via evaluation of inter-spike interval histograms and cross-correlations. Putative units with less than 30 spikes or refractory periods $\leq$ 1ms were discarded.

Kilosort (https://www.biorxiv.org/content/10.1101/061481v1) was used for spike sorting of the chemogenetic dataset because its automatic drift correction allowed assessment of the firing rates of the same units during baseline recordings and the recordings after CNO injection. First, baseline recordings and recordings after CNO injection were spliced. Next, Kilosort2 (https://github.com/MouseLand/Kilosort) with default parameters was used for automatic spike sorting of the spliced recording. The results of automatic spike sorting were then manually curated using Phy software (https://github.com/cortex-lab/phy) by an expert reviewer (EM). Finally, a second expert reviewer (CA) inspected the quality of clusters curated by the first reviewer before further analysis. The reviewers evaluated the quality of clusters based on their waveforms and correlograms.

Analysis of single unit and LFP data was performed using custom MATLAB scripts. After identification of single units, the firing rate for each unit and distribution of spike amplitudes and widths were derived from the baseline recordings. For firing rates, the number of spikes during the baseline recording period was divided by the total duration of this period. Spike amplitudes were defined as the maximum positive amplitude of spike waveforms. The spike width was calculated as the time between the point where a spike reached 50% of its maximal amplitude prior to the peak and the point where the spike returned to 50% of its maximal amplitude after the peak. Depths of each unit were determined based on the average depth of the 4 contacts contributing to the tetrode where a unit was recorded.

To identify light-responsive units, peri-stimulus time histograms (PSTHs) were generated by aligning spike times to the time when the flashing screen turned, generating a distribution of spikes relative to the onset of the light stimulus for each unit. PSTHs were manually reviewed to identify units that demonstrated a clear increase in firing following stimulus onset.

After applying a 0.1 Hz–4000 Hz bandpass filter to the LFPs, the LFPs were time-locked to light stimulus onset and averaged across trials to generate ERPs. The channel that displayed the ERP with the maximum amplitude for each unit was plotted on the PSTH for that unit to observe for relationships between single unit activity and the LFP evoked by the light stimulus.

The responsiveness of single units to a particular direction or orientation of drifting grating was used as a measure of the functional integration of transplanted neurons with the visual network. Orientation selectivity index (OSI) for each unit was calculated using the equation below where F(c θ) is the firing rate at a given presentation angle.[65]

$$\sum \frac{F(\theta)e^{2i\theta}}{F(\theta)}$$

QUANTIFICATION AND STATISTICAL ANALYSIS

For analysis of immunohistological data, a non-parametric Kruskal-Wallis ANOVA was used to compare data across multiple timepoints. Pairwise comparisons were then performed using Dunn's test. For analysis of electrophysiological data, an ANOVA was performed to assess for a relationship between post-transplantation timepoint and organoid versus naive visual cortex recordings

on the number of units detected. To assess for the effect of depth, timepoint, and organoid versus naive visual cortex recordings, a generalized estimator equation was fit to the firing rate, spike amplitude, and spike width. Unit depths were normalized as a percentage of the total organoid depth at a given track. The Wilcoxon matched-pairs signed rank test was used to compare firing rates in the chemogenetic experiments. A p value of 0.05 was used as the threshold for significance. Software packages used for statistical analysis included R (version 4.1.2) and OriginPro (version 2022; OriginLab Corporation).